“ALEXANDRU IOAN CUZA" UNIVERSITY OF IAȘI
FACULTY OF CHEMISTRY
DOCTORAL SCHOOL OF CHEMISTRY

Short peptides with self-assembly properties: synthesis, characterization, and potential applications

PhD THESIS SUMMARY

PhD supervisor,
Prof. univ. dr. **Gabi DROCHIOIU**

PhD student,
Chem. **Ștefania-Claudia Jitaru**

IASI
2025

DOCTORAL COMMITTEE MEMBERS

President:

PhD supervisor:

Prof. univ. dr. **Gabi DROCHIOIU**

"Alexandru Ioan Cuza" University of Iași

Scientific referees:

ACKNOWLEDGEMENTS

First of all, I would like to express my sincere gratitude to my scientific advisor, ***Prof. univ. dr. Gabi Drochioiu****, for the guidance and support provided throughout my doctoral studies.*

I would also like to thank the members of the advisory committee, ***Prof. univ. dr. Aurel Pui, Conf. univ. dr. Robert Grădinaru****, and* ***CS III Dr. Dana Suflet****, for their valuable observations, constructive criticism, and support in shaping this doctoral thesis.*

I am especially grateful to ***Conf. univ. dr. habil. Brîndușa - Alina Petre,*** *and* ***Conf. univ. dr. Robert Grădinaru*** *for their close collaboration, constant guidance, patience, and support over all these years.*

I also wish to thank ***Dr. Laura Darie-Ion*** *and* ***Dr. Cosmin Ștefan Mocanu*** *for sharing their knowledge and providing training within the Biochemistry Laboratory. At the same time, I would like to express my gratitude to* ***Dr. Olga Pintilie*** *and* ***Chem. Elena Mihalcea*** *for their moral support.*

I thank ***Dr. Iuliana Stoica*** *for her support in the analysis and evaluation of samples using AFM, which added significant value to the research presented in this thesis.*

I wish to thank ***Conf. univ. dr. Andrei Neamțu*** *și* ***Dr. Cornel Cojocaru*** *for their collaboration and valuable expertise in computational studies, which contributed significantly to obtaining new perspectives in relation to the experimental results.*

I am grateful to ***Dr. Dumitrela Diaconu*** *and* ***Dr. Violeta Mangalagiu*** *for their assistance in acquiring ESI-MS spectra data. In addition, I wish to thank* ***Chem. Alexandru Puiu*** *for his generosity in providing the FEHNF peptide used in preliminary studies on the self-assembly process.*

I also thank the ***POCU/993/6/13/153322*** *project, which facilitated collaboration through an internship with* ***Dr. Andra-Cristina Enache*** *from the "Petru Poni" Institute of Macromolecular Chemistry (ICMPP), to whom I am extremely grateful for her dedication as a mentor.*

Last but not least, I thank the colleagues from the ***TRANSCEND center at the Regional Oncology Institute in Iași,*** *those from the* ***"Petru Poni" Institute of Macromolecular Chemistry (ICMPP) in Iași****, and the* ***Integrated Center for Environmental Science in the North-East Region – CERNESIM****, for access to infrastructure.*

TABLE OF CONTENTS

INTRODUCTION

In recent years, oligopeptides have gained increasing importance in fields such as biology, chemistry, and medicine, attracting the attention of the scientific community due to their remarkable characteristics, ranging from antibacterial properties to photoactive behaviors (Abbas et al., 2022; Sun et al., 2019). Ultra-short peptides, defined as having up to 7 amino acids, are being studied in particular for their ability to facilitate targeted drug delivery and release (Apostolopoulos et al., 2021; Yang et al., 2023). In addition, the distinct properties of short peptides give them high potential for a wide range of applications, such as the creation of matrices for cell cultures (Restu et al., 2020), tissue regeneration processes (Ross et al., 2022), and biosensor development (Sfragano et al., 2021). Recent studies have highlighted the importance of short peptides in advanced gene therapy (Riley and Vermerris, 2017).

The main objectives of the thesis "*Short peptides with self-assembly properties: synthesis, characterization, and potential applications*" were as follows:

O1. Selection of a peptide sequence inspired by natural sequences and its synthesis by solid-phase method, in order to study its self-assembly properties.

O2. Synthesis of tyrosine mutant variants from the selected peptide with self-assembly properties, in order to evaluate its influence on the self-assembly mechanism.

O3. Optimizing the purification and separation of the peptides obtained by reverse-phase high-performance liquid chromatography and reverse-phase solid-phase extraction.

O4. Characterization of peptides by advanced analytical techniques, such as MALDI-ToF mass spectrometry, tandem mass spectrometry, and ESI-MS mass spectrometry, in order to confirm the molecular weight, purity, and structural integrity of the compounds obtained.

O5. Determination of the spectral characteristics of the FESNF peptide through UV-vis and spectrofluorimetry studies, as well as investigation of its ability to aggregate and form complexes with Cu(II) ions.

O6. Investigation of the self-assembly process of newly synthesized peptides using microscopic techniques such as atomic force microscopy (AFM), polarized optical microscopy (POM), and transmission electron microscopy (TEM).

O7. Further research into the self-assembly mechanism of the FEYNF peptide through Fourier transform infrared spectroscopy (FTIR) and spectrofluorimetric studies.

O8. Use of complementary methods, such as *in silico* studies, to deepen the understanding of peptide self-assembly mechanisms and investigate potential biomedical applications.

O9. Dissemination of results by publishing them in recognized scientific journals with impact factor and by participating in international and national conferences.

PART TWO. PERSONAL CONTRIBUTIONS

II. SELF-ASSEMBLING PEPTIDE FESNF-NH_2

The pentapeptide FESNF–NH_2 was selected for the study of self-assembling properties due to its potential to form organized structures through specific interactions between its constituent amino acid residues and its biological relevance. **Figure II.1** shows the localization of the FESNF peptide sequence both within hen egg-white lysozyme (region 34–38) and in the CHAMP1 protein (region 772–776). Hen egg-white lysozyme exhibits a structure highly similar to that of human lysozyme, which has the ability to self-assemble into amyloid fibrils and is implicated in the onset of amyloid diseases. Consequently, it has been frequently used in vitro as a model protein for studying fibril formation (Wang et al., 2021). Furthermore, mutations in the CHAMP1 gene have been associated with a rare form of intellectual disability.

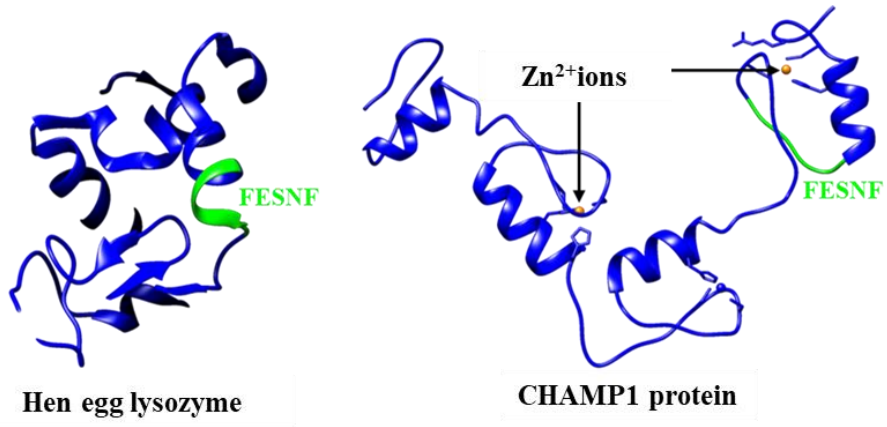

Figure II.1. Structural representations of hen egg-white lysozyme (left, PDB: 1DPX) and the CHAMP1 protein (right, F1MFQ9, SWISS-MODEL) obtained using UCSF Chimera version 1.14. The region containing the FESNF sequence is highlighted in green, while zinc ions are shown in orange.

II.2. SYNTHESIS, PURIFICATION, AND CHARACTERIZATION

II.2.1. High-performance liquid chromatography analysis

The pentapeptide FESNF was successfully obtained using solid-phase peptide synthesis (SPPS) and purified by reversed-phase high-performance liquid chromatography (RP-HPLC). Initial HPLC analysis revealed two compounds (**Figure II.2.1**, left), indicating the presence of the peptide of interest and a secondary synthesis product (Jitaru and Drochioiu, 2023). The initial purity of the crude peptide was estimated at 79% and 77%, based on the signals recorded at 215 nm and 220 nm, respectively. The elution of the secondary product occurred approximately two minutes after the elution of the target peptide, suggesting a more pronounced hydrophobic character. After two rounds of purification, the peptide purity increased to 96% (**Figure II.2.1**,

right). Subsequently, the molecular weight of the purified peptide and the secondary product was analyzed using matrix-assisted laser desorption/ionization time-of-flight mass spectrometry (MALDI-ToF MS) and MALDI-ToF/ToF.

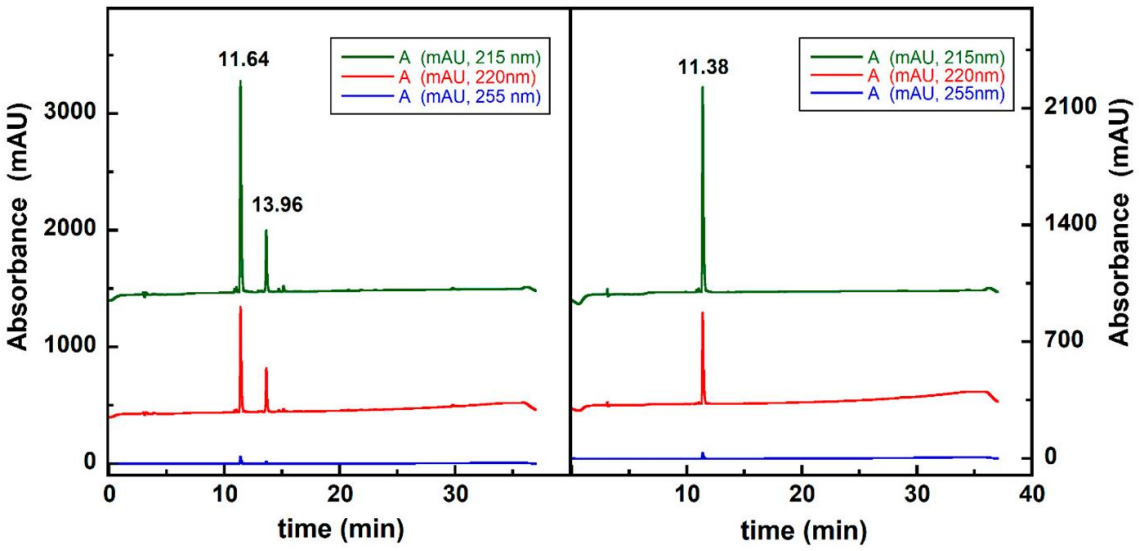

Figure II.2.1. HPLC chromatograms of the crude peptide (left) and purified FESNF peptide (right), obtained by monitoring at three wavelengths (215, 220, and 255 nm).

II.2.2. MALDI-ToF mass spectrometry analysis

The molecular weight and purity of the peptide were determined by mass spectrometry using MALDI-ToF and MALDI-ToF/ToF methods (**Figure II.2.2**). MS analysis of the compound eluted at a retention time of 11.64 min confirmed the successful synthesis of the FESNF-NH_2 peptide. Initially, the sample was co-crystallized with the HCCA and DHB matrices for MALDI-ToF analysis. The mass spectra obtained showed more intense signals when using the DHB matrix, indicating higher ionization efficiency. Moreover, the crystals formed with DHB were larger in size, suggesting more favorable conditions for spectrometric analysis (**Figure II.2.2**).

The mass spectrum indicated the presence of the molecular ion $[M+H]^+$ at m/z 642.48. Sodium ($[M+Na]^+$) and potassium ($[M+K]^+$) adducts were also observed at m/z 664.46 and m/z 680.44, respectively (**Figure II.2.3**). The experimental values were compared with theoretical values calculated using GPMAW software. Furthermore, peptide sequence analysis by MS/MS was used to confirm the primary structure of the FESNF-NH_2 peptide.

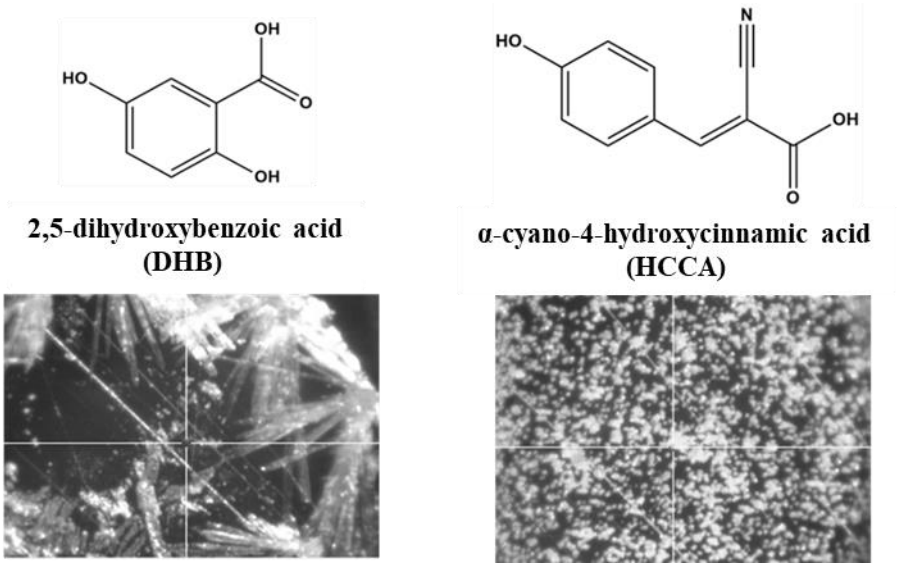

Figure II.2.2. Visual comparison of the co-crystallization of the FESNF-NH_2 peptide with two different matrices: DHB and HCCA. Images were captured using the camera of the MALDI-ToF mass spectrometer.

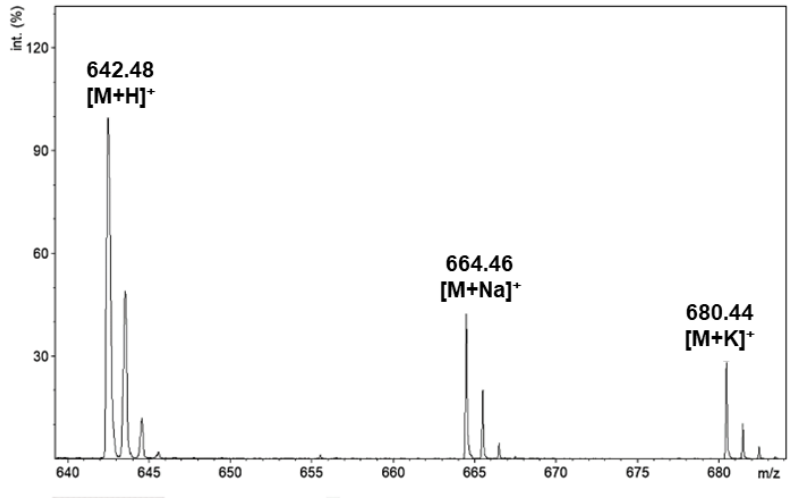

Figure II.2.3. MALDI-ToF mass spectrum of the FESNF peptide obtained using the DHB matrix.

II.2.2.1. Tandem mass spectrometry analysis

As expected, fragmentation of the molecular ion of the peptide of interest at m/z 642.48 generated several singly charged b^+ and y^+ ions, as well as species resulting from the loss of neutral molecules such as water (H_2O), ammonia (NH_3), and carbon dioxide (CO_2) (**Figure II.2.4**). The structural fragmentation pattern of the FESNF peptide can be observed in **Figure II.2.5**. The loss of water can be attributed to glutamate and serine residues, while the 17 Da deviation associated with ammonia release may be attributed to the N-terminal of the pentapeptide or the release of water combined with an isotopic shift (Sun et al., 2008). For the y^{2+}, y^{3+}, and b^{4+} fragments, the loss of ammonia could originate from the free amino group on the

side chain of asparagine (Tabb et al., 2006). On the other hand, the loss of carbon dioxide, observed both for the molecular ion and its dehydrated species, may result from decarboxylation of the glutamate residue (Jackson et al., 2011).

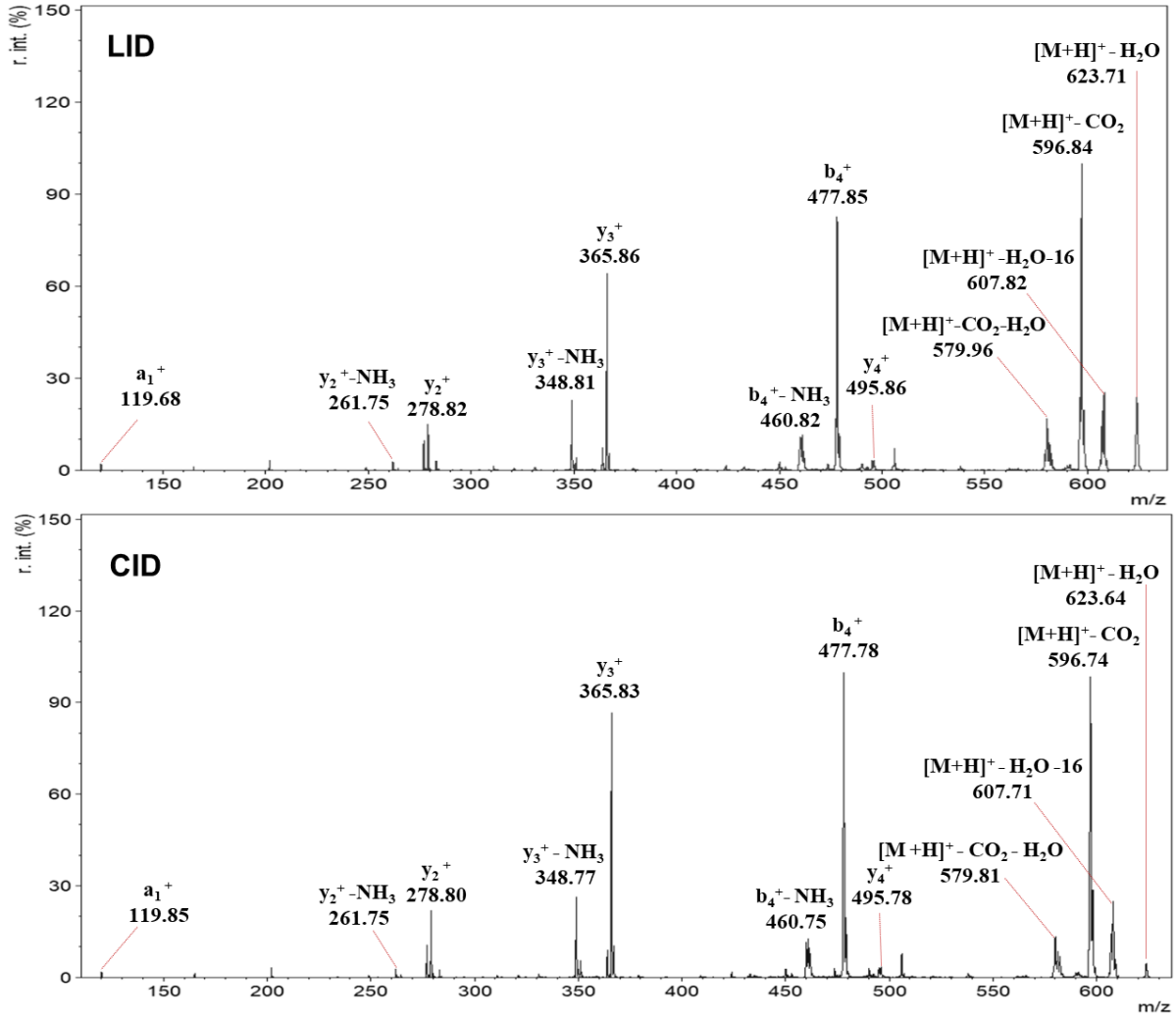

Figure II.2.4. Assignment of m/z signals resulting from tandem mass spectrometry analysis of MALDI-ToF MS/MS type, using the DHB matrix. The fragmentation of the molecular ion [FESNF + H]$^+$ (m/z 642) was achieved through laser-induced dissociation (LID) and collision-induced dissociation (CID) respectively (for the fraction collected at 11.64 minutes in the RP-HPLC chromatographic separation).

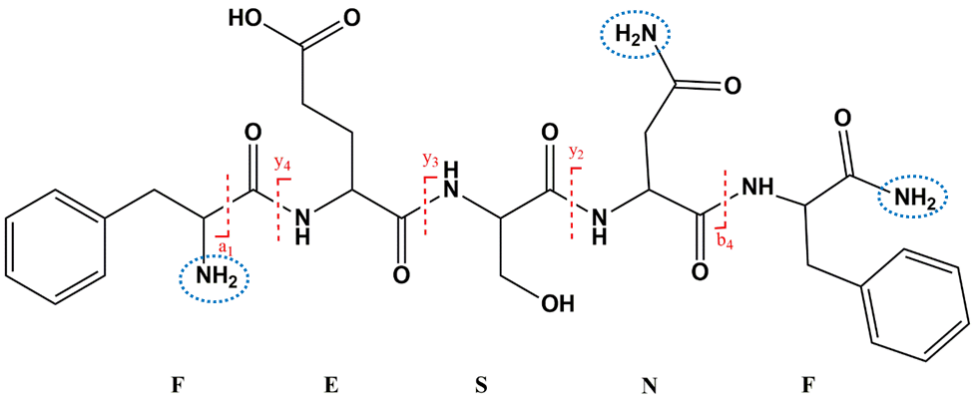

Figure II.2.5. Highlighting the preferential fragmentation types observed experimentally in the case of the FESNF-NH_2 pentapeptide upon tandem mass spectrometry analysis.

II.2.3. Analysis by electrospray ionization mass spectrometry

The ESI-MS mass spectrum (**Figure II.2.9**) confirms the identity of the FESNF-NH_2 peptide, with the most intense signal corresponding to the molecular ion ($[M+H]^+$) at m/z = 649.28. The spectrum also indicates the presence of sodium adducts $[M+Na]^+$ at m/z = 664.26 and potassium adducts $[M+2K-H]^+$ at m/z = 718.31. In addition, the signal at m/z = 1283.56 ($[2M+H]^+$) indicates the intrinsic tendency of the peptide to form dimers (Pan, 2008).

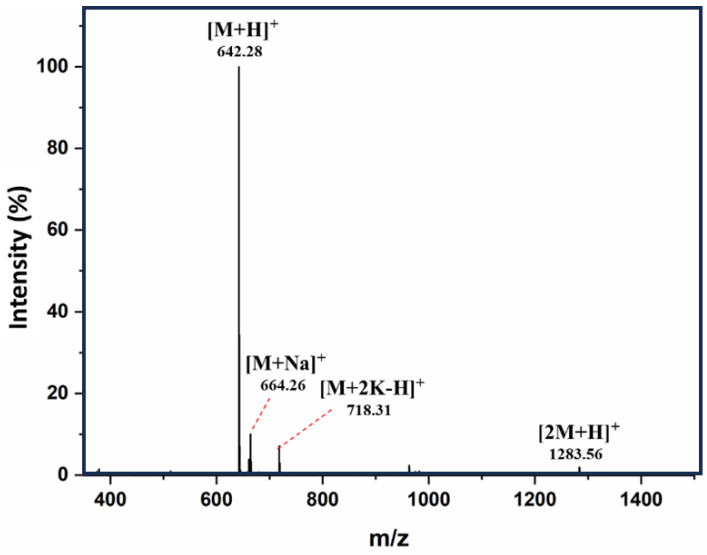

Figure II.2.9. ESI-MS mass spectrum of the FESNF-NH_2 peptide.

II.3. SPECTRAL STUDIES

Spectroscopic analysis of the FESNF-NH_2 peptapeptide reveals two characteristic signals, attributed to phenylalanine residues at the N- and C-terminals. The presence of aromatic amino acids may favor the self-assembly process of the peptide. To evaluate the potential

involvement of the peptide in interactions with metal ions, the presence and behavior of aromatic residues were analyzed by UV-vis spectroscopy and spectrofluorimetry.

The UV-vis spectrum of the peptapeptide was recorded in Tris buffer solution to establish the characteristic fingerprint of phenylalanine residues. Thus, the most intense peak observed at 258 nm was accompanied by four spectral shoulders at 247, 252, 263, and 267 nm, both at pH 7.3 and pH 7.0 (**Figure II.3.1**). A similar spectroscopic profile was observed using 30 mM PIPES buffer solution, pH 6.5, at a peptide concentration of 200 µM. These results are consistent with previously reported data for phenylalanine-containing peptides (Barazzouk and Daneault, 2012; Rodger, 2018). The diluted peptide solution (41 µM) exhibits a spectral band characteristic of the amide group at 203 nm (A_{203} 0.97) under conditions of pH 7.3. Phenylalanine can act as an intermediate for electron transfer between distant regions of the peptide structure (Nathanael et al., 2018). The modest contribution of phenylalanine to the intrinsic fluorescence of the peptide can be explained by its low quantum yield (Lakowicz, 2006).

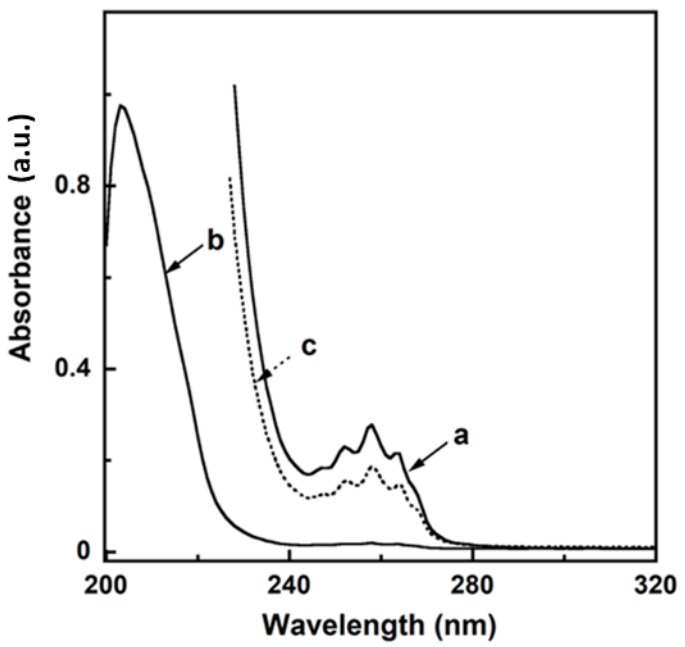

Figure II.3.1. UV-vis spectra of the pentapeptide FESNF in Tris 30 mM pH 7.3 (a and b, 826 µM and 41 µM) and acetate 40 mM pH 7.0 (600 µM, spectrum c, dotted).

At the same time, spectrofluorimetric measurements highlight spectral features specific to peptides containing phenylalanine residues. The emission spectrum of the FESNF-NH_2 peptide in 30 mM Tris buffer solution, pH = 7.3, at an excitation wavelength of 258 nm, shows a maximum at 282 nm and a shoulder at 290 nm. Good linearity between the fluorescence signal intensity and the peptide concentration can be observed in the concentration range 25–250

μg/mL at an emission wavelength of 282 nm (**Figure II.3.2** - Insert). Similarly, the emission spectrum of the peptide in 50 mM sodium acetate, pH = 5.05, was measured and a similar profile was found. As expected, the excitation spectra show a maximum at 258 nm (**Figure II.3.3** - *dotted spectra*).

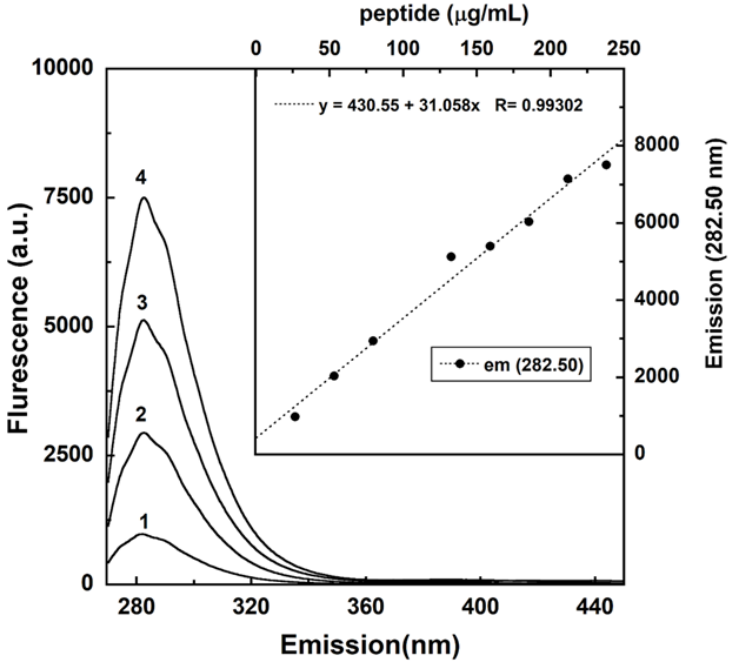

Figure II.3.2. Emission spectra of the peptide FESNF-NH_2 (1, 2, 3, and 4 at 26, 80, 132, and 238 μg/mL) in 30 mM Tris buffer, pH 7.3. *Insert:* fluorescence intensity as a function of peptide concentration.

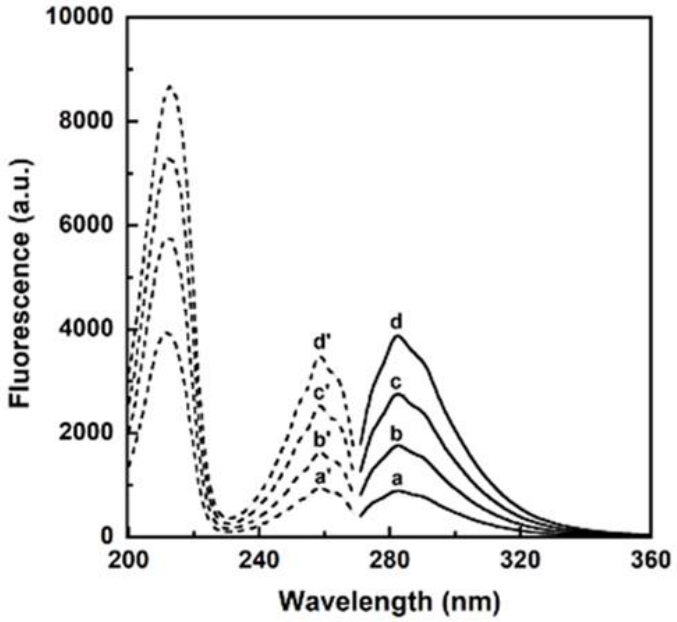

Figure II.3.3. Emission spectra at four different peptide concentrations (39, 78, 132, and 176 μM – a, b, c, and d; solid lines) obtained for $\lambda_{excitation}$ = 258 nm and the corresponding excitation spectra (a', b', c' and d'; dashed lines) recorded at $\lambda_{emission}$ = 282 nm, in 50 mM sodium acetate solution, pH = 5.05.

II.4. AGGREGATION STUDIES

Typically, the physical stability of peptides and proteins is influenced by several factors. The ability of a peptide to form aggregates can be influenced by the amino acid sequence, the net charge of the peptide, and its concentration (Zapadka et al., 2017).

The aggregation index (AI) is an important parameter that indicates the tendency of a peptide to form aggregates in solution, especially when its value is greater than 3. Phenylalanine has been shown to have the ability to form fibrils in PBS at 37°C (Anand et al., 2017). Furthermore, the presence of phenylalanine residues in hexapeptides, in cross-folded β-structured aggregates, and in amyloid-like species has been previously reported in the literature (Rousseau et al., 2006), and the tendency to aggregate is strongly influenced by the number of these amino acid residues in the molecule (Zaguri et al., 2021). On the other hand, asparagine and glutamine may play an important role in initiating the aggregation process of peptides and proteins (Barrera et al., 2021; Shattuck et al., 2017).

As expected, the aggregation index obtained was greater than 40 when the absorbance at a wavelength of 280 nm was used at pH 6.00, 8.00, and 10.7. These values, calculated according to equation 1, apply mainly to aggregation studies performed on proteins. In contrast, more relevant results for the pentapeptide studied were obtained when the AI had low values (below 3), calculated based on the absorbances recorded at wavelengths of 258 and 350 nm. The dynamic aggregation profile is shown in **Figure II.4.1.** The maximum AI value (2.8) was obtained at pH 6 after 20 minutes of incubation at 37 °C.

Similarly, the aggregation of the pentapeptide was investigated at pH 2. Under these conditions, it was interesting to note that a plateau was reached after 30-40 minutes of incubation using a 2 mg/mL peptide solution. The aggregation index was also determined as a function of pH after 30 minutes of incubation at 37 °C. The bell-shaped profile obtained (**Figure II.4.1**, inset) clearly suggests that the FESNF peptide favors a slightly acidic environment to initiate the aggregation process.

The aggregation capacity of the peptide was also investigated using the ThT test. Phenylalanine forms aggregates, and the intensity of ThT fluorescence increases due to the capture of the dye by the structures resulting from self-assembly (Ziaunys and Smirnovas, 2019). In this case, it is possible that the results are influenced by the total electric charge of the FESNF-NH_2 peptide. Thus, after an incubation period of 145 hours at 50 °C, an 18% increase in fluorescence was observed at pH 8 (**Figure II.4.2**). The electrostatic interaction between ThT, which is positively charged, and the partially negative peptide under investigation may intensify

the fluorescence signal. Electrostatic interactions between fibrils and ThT are the main factor determining fluorescence intensity (Arad et al., 2020).

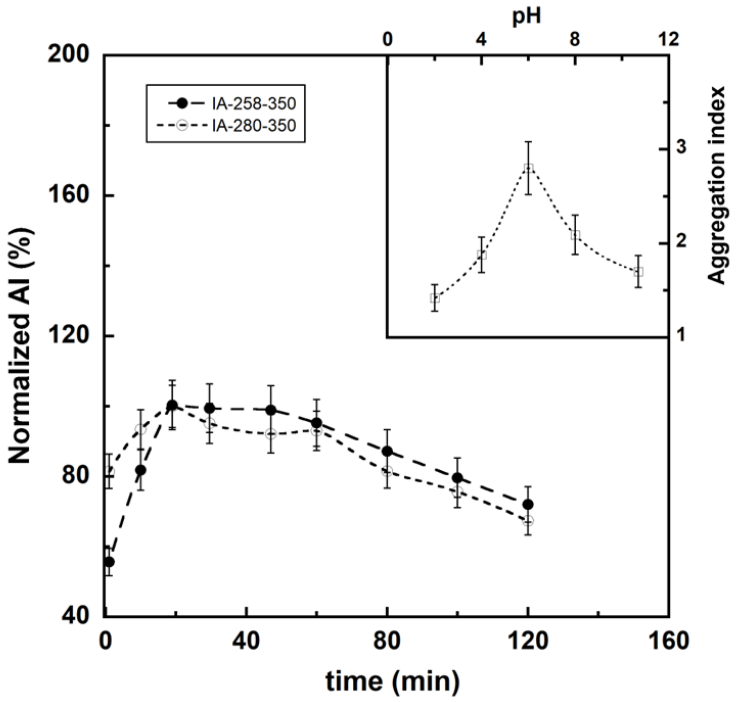

Figure II.4.1. Normalized aggregation index (AI) calculated based on absorbance values at 258 nm and 280 nm, respectively 350 nm. The maximum AI values were 2.8 (solid dots) and 44 (empty dots), respectively. *Insert:* variation of the aggregation index (AI) as a function of pH values.

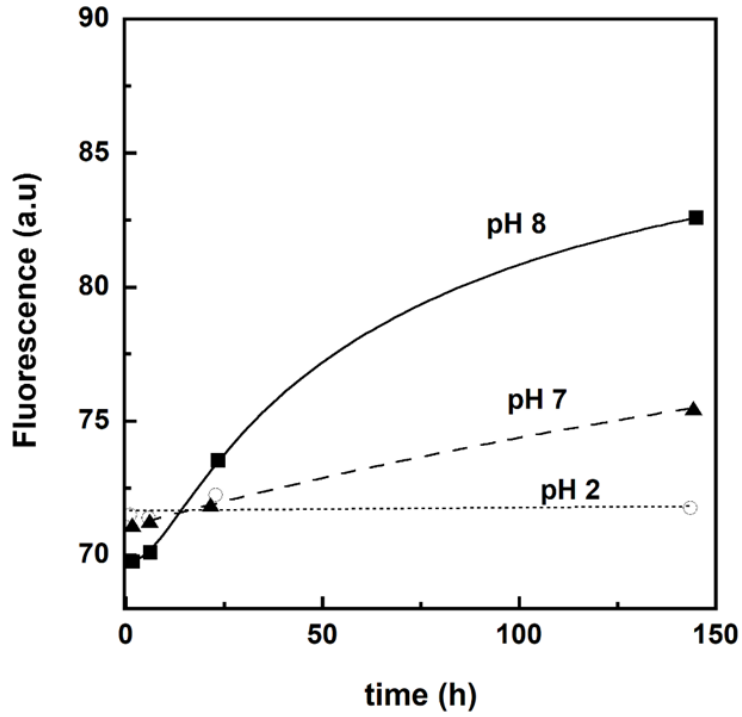

Figure II.4.2. Increase in emission signal intensity ((λ_{ex} 440 nm and (λ_{em} 482 nm) of thioflavin (40 µM ThT) in the presence of pentapeptide at pH 8.0 (■), pH 7.0 (▲), and pH 2.0 (○), as function of the incubation time at 50 °C.

II.5. STUDY OF SELF-ASSEMBLY PROPERTIES BY AFM

The morphology of the aggregated species derived from FESNF-NH_2 in different solution media was analyzed using atomic force microscopy (AFM) and presented in **Figure II.5.1**. The ammonium acetate solution with pH 5.5 and the methanol solution (**Figure II.5.1**, A, A', and D, D', respectively) appear to induce a fibril agglomeration effect. This effect is more noticeable in **Figure II.5.1** D, D', and D", which once again confirms that short-chain alcohols induce a delay in fibril formation, as previously described in another similar study (Bernson et al., 2020). In addition, it has been reported in the literature that methanol substantially modifies the morphology of compounds by significantly decreasing the drying time (Zelenovskiy et al., 2015).

The fibrils observed in the sample obtained in the presence of ammonium acetate at pH 5.5 resemble a neural network. In this case, the average width of the fibrils is approximately 130 nm, compared to that of the fibrils obtained for the sample obtained from the methanol solution, where the average width is greater, around 235 nm, as can be seen from the measurements based on the cross-sectional profiles in **Figure II.5.1** A" and D", respectively.

The theoretical isoelectric point (pI) of the FESNF-NH_2 peptide is 6.99, as calculated using the BACHEM Peptide Calculator. At a physiological pH of 7.4, which is close to the pH value corresponding to the isoelectric point (pI), no peptide fibrils are formed (Liu et al., 2022) (**Figure II.5.1** B and B'). Instead, dense clusters ranging in size from 116 to 128 nm were formed, depending on the cross-sectional profile (**Figure II.5.1** B"). This behavior is similar to that exhibited by bovine insulin when exposed to a pH close to its isoelectric point (Bernson et al., 2020). Furthermore, the appearance of amyloid fibrils in the case of Alzheimer's disease peptides tends to be favored when the net electric charge is zero due to pH conditions (Guo et al., 2005).

However, at pH 8.2, the pentapeptide self-assembles into long, homogeneous, and distinct nanofibrils (**Figure II.5.1** C and C'), with an average width of approximately 165 nm (see cross-sectional image in **Figure II.5.1** C"). Furthermore, salts can facilitate fibril formation at pH 8.2 due to the predominance of negative charges (Hong et al., 2004). By deprotonating the glutamic acid residue, intra- and intermolecular interactions can be enhanced, particularly hydrogen bonds mediated by the side chains of glutamic acid, serine, and asparagine in the main structure of the peptide. Implicitly, π-π intermolecular interactions may become more pronounced. Under these conditions, the pentapeptide self-assembles near the pKa value of the Tris buffer, forming long, homogeneous, and distinct nanofibers (**Figure II.5.1** C, C') with an average width of approximately 165 nm (cross-sectional profile **Figure II.5.1** C"). Therefore, it

is important to take into account the contribution of partially dissociated -NH_2 groups originating both from the N-terminal end of the peptide and from the buffer solution.

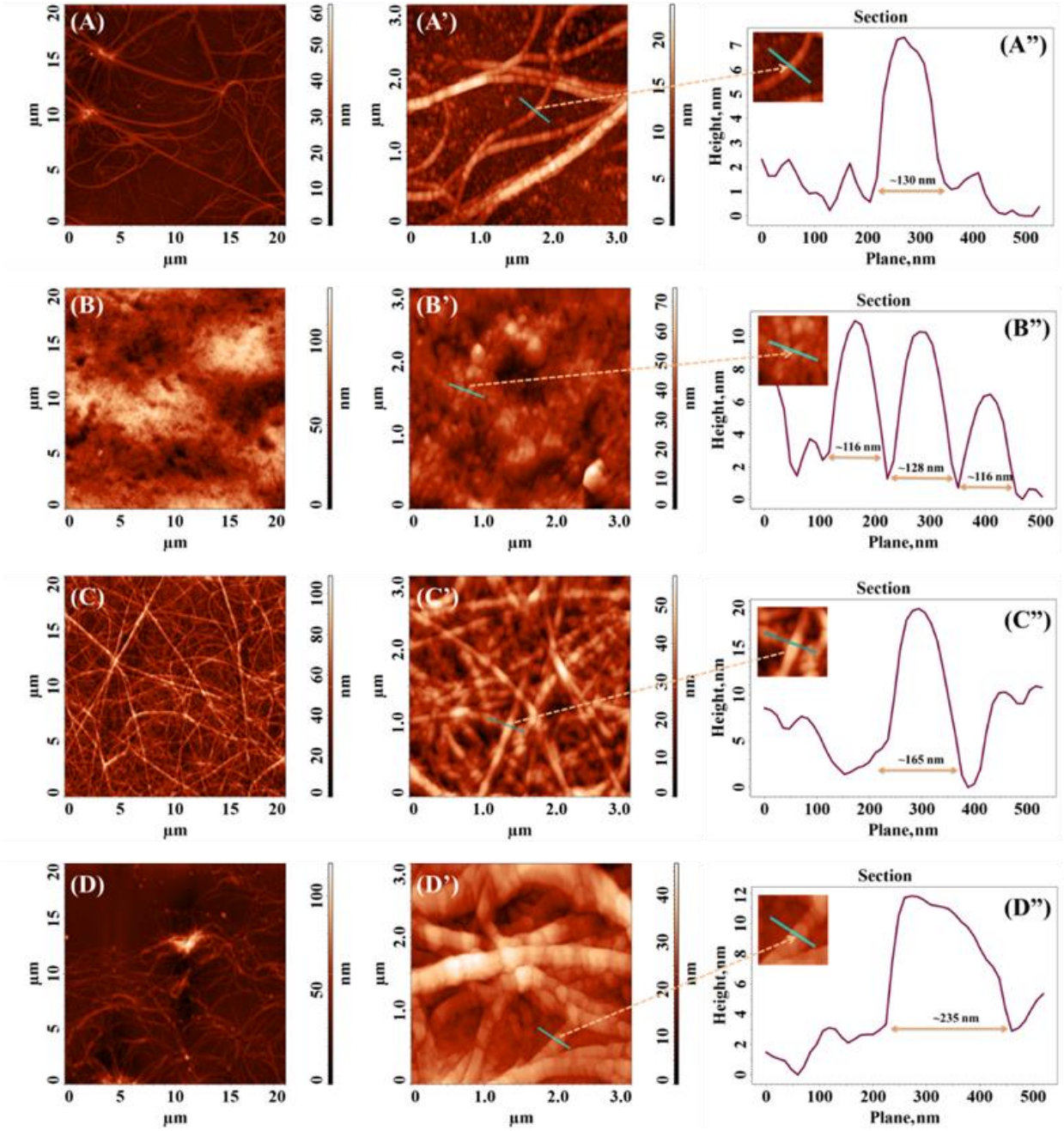

Figure II.5.1. Two-dimensional (2D) AFM images recorded on surfaces of 20x20 μm^2 and 3x3 μm^2, respectively, and the corresponding cross-sectional profiles of samples obtained from the aqueous solution FESNF-NH_2 (10 mg/mL) diluted in a 1:10 ratio using (A, A', A") ammonium acetate 50 mM pH 5.5; (B, B', B") Tris 50 mM pH 7.4; (C, C', C") 50 mM Tris pH 8.2; (D, D', D") 4.5% methanol solution.

The fibrils appear to be the result of several globular structures stacked together, as can be seen in the enlarged image in the corner of the height profile (**Figure II.5.1** C"). These results are consistent with a recent study in which a sensor was developed for the detection of

verbascoside in various types of olive oil by immobilizing the FESNF-NH_2 peptide using glutaraldehyde as a cross-linking agent on screen-printed carbon electrodes modified with graphene oxide. This study also observed a fibrillar peptide network within the sensor (Munteanu et al., 2022). Thus, the Tris solution can act as a trigger for the formation of more developed 3D structures. In addition, another study observed a regular and dense network of small-diameter fibers (4–5 nm) in the case of the FEFEFKFK peptide, through AFM and TEM analysis (Saiani et al., 2008).

In conclusion, AFM analysis clearly shows the self-assembly ability of the peptide through the formation of aggregate species depending on pH. The correlation between the aggregation index and AFM images confirms the significant influence of pH on the self-assembly process.

II.6. *IN SILICO* STUDIES

II.6.1. Replica exchange molecular simulations

The study in this thesis focused mainly on investigating the possibility that phenylalanine residues at the ends of the peptide participate in intramolecular π-π interactions. The research was initiated based on the hypothesis that the preference for this conformation limits the extensive aggregation caused by hydrophobic interactions, due to steric interference between adjacent molecules. The results of replica exchange simulations of the isolated peptide showed that, regardless of the pH value, the peptides predominantly adopt an extended ("open") conformation, in which the aromatic side chains of the phenylalanine residues are positioned at a distance from each other (**Figure II.6.1** A). The histograms of the distance between the C_γ–$C_{\gamma'}$ carbon atoms of the Phe1 and Phe5 residues at the ends of the molecule show a small number of "closed conformations," which involve π-π intramolecular interactions (**Figure II.6.1** B).

Simulations with two peptides showed that π-π interactions between the side chains of the terminal phenylalanine residues are predominant in the conformation of the assembly (**Figure II.6.1** D). These interactions are possible because the terminal ends remain available and are able to interact with other molecules. It is interesting to note that the presence of the second molecule influences the intramolecular conformational preference of each peptide. The histogram of the distance between the C_γ–$C_{\gamma'}$ carbon atoms at the ends of the molecule shows a second peak around ~6 Å (**Figure II.6.1** C), compared to a single dominant peak centered at ~12 Å in the single-peptide simulations. This increased tendency toward a "closed" conformation can be explained by simultaneous π-π interactions, both intramolecular and intermolecular (**Figure**

II.6.1 D). The results suggest that "open" structures favor aggregation, allowing the terminal ends to remain free for hydrophobic interactions involved in aggregate growth.

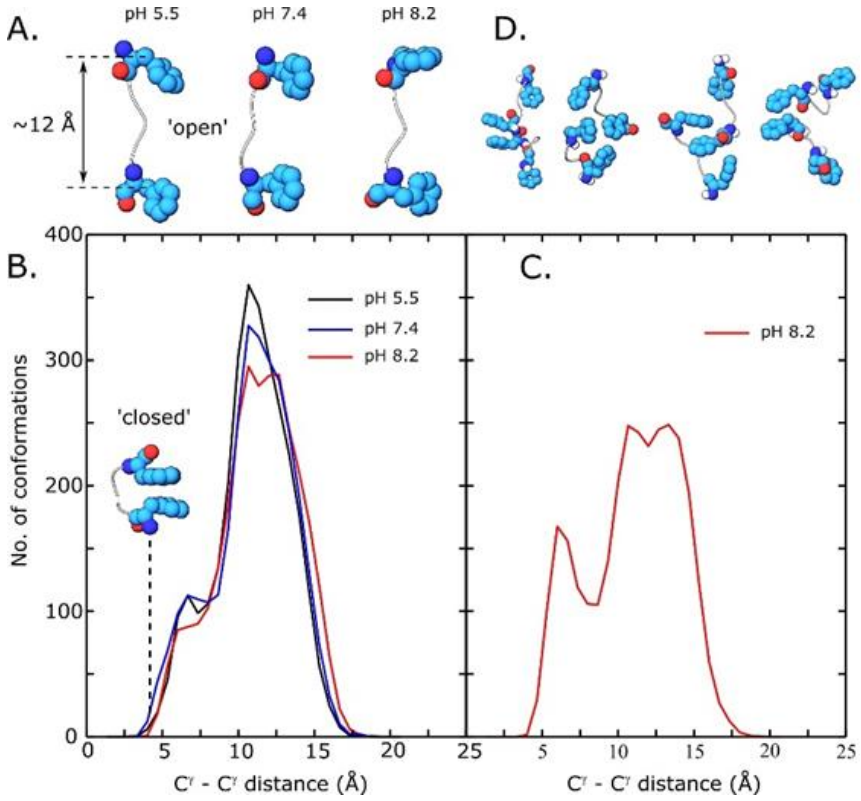

Figure II.6.1. Conformational analysis based on REST2 simulations for a single peptide (A, B) and for two peptides (C, D). A – dominant conformation extracted from cluster analysis at acidic, neutral, and slightly basic pH; B – histogram of the distribution of distances between Cγ–Cγ' carbon atoms at the chain ends (terminal phenylalanine residues) in single-peptide simulations; C – histogram of the distribution of C_{γ}–$C_{\gamma'}$ distances between chain ends in two-peptide simulations; D – conformations of peptide dimers extracted from simulations with two peptides.

II.6.2. Coarse-grained molecular simulations

To investigate the aggregation tendency of the FESNF peptide in more detail, coarse-grained (CG) molecular simulations were performed. In this type of simulation, chemical groups consisting of several atoms are represented by a single interaction center. This method allows the simulation to be run for periods at least 10 times longer, which provides a broader picture of slow molecular processes such as aggregation. **Figure II.6.2** A shows the result of a CG simulation run over a period of 0.8 μs, which included 400 FESNF peptides at pH 8.2. At the beginning of the simulation, the peptides were randomly distributed throughout the simulation box. During the simulation, the molecules gradually self-assembled into larger and larger aggregates, eventually forming a fibrillar structure, as illustrated in **Figure II.6.2** B.

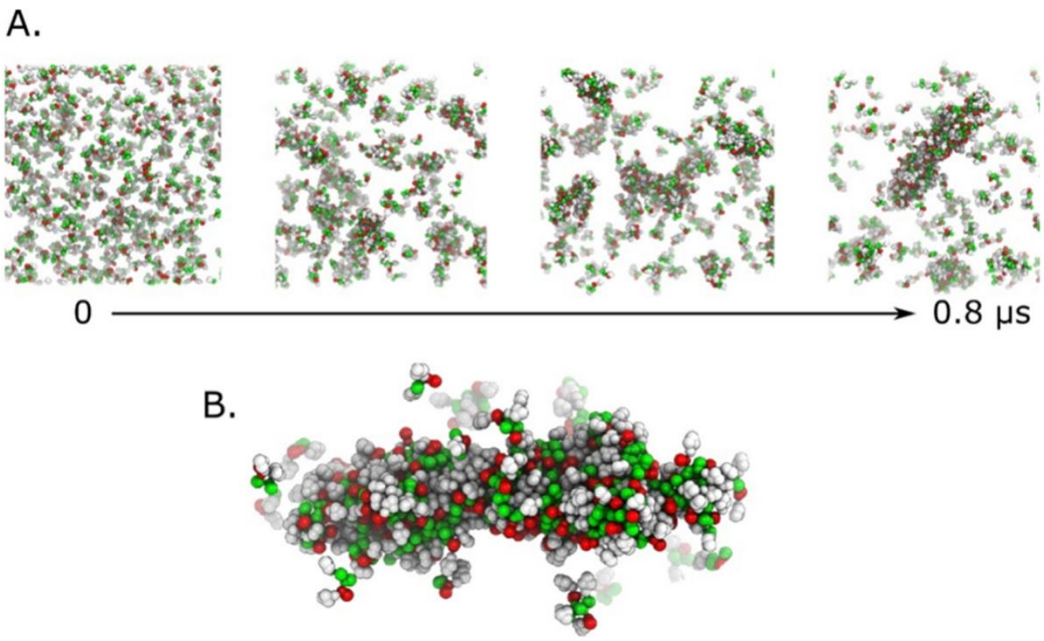

Figure II.6.2. Coarse-grained (CG) simulation of the self-assembly of the FESNF-NH_2 peptide at pH 8.2. A - time series of peptide aggregate growth; B - fibrillar aggregate formed after ~0.8 μs.

II.7. INTERACTION OF PEPTIDE WITH COPPER (II) IONS

II.7.1. UV-vis studies

The UV-vis spectra of the pentapeptide FESNF in the presence of a 30 mM PIPES (1,4-piperazinediethanesulfonic acid) buffer solution at pH = 6.5 indicate a distinct interaction with Cu^{2+} ions. In the absence of metal ions, the peptide exhibits two absorption maxima, at 220.5 nm and 258 nm, with an $A_{220.5}/A_{258}$ ratio of 12.6. The absorption at 258 nm is predominantly attributed to the presence of characteristic aromatic rings, phenylalanine (F) residues, in the peptide sequence, while the maximum at 220.5 nm reflects the contribution of the four peptide bonds and the amide group located at the C-terminal end (**Figure II.7.1**) (Prasad et al., 2017).

As the concentration of Cu^{2+} equivalents increases (**Figure II.7.1**, spectra b-e), a progressive increase in absorption in the UV region is observed, accompanied by a significant shift in the absorption maximum. This change indicates the formation of a complex between the peptide and Cu^{2+} ions. The Cu^{2+} ions most likely bind to peptide groups and/or functional groups located in the side chains of the component amino acids (such as the carboxyl group of glutamic acid, the hydroxyl groups of serine, or the amide nitrogen), interfering with the chromophore groups (Faller, 2009).

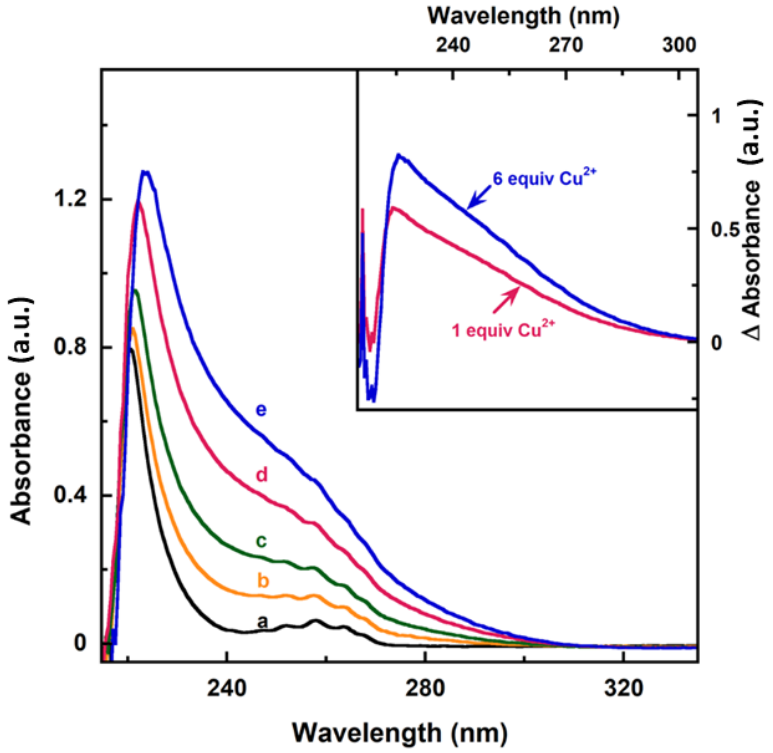

Figure II.7.1. UV-vis spectra of the FESNF-NH_2 peptide in the absence or presence of different concentrations of $CuSO_4$ solutions. *Conditions:* 30 mM PIPES, pH= 6.5. The peptide exhibits two absorption maxima at 220.5 and 258 nm (a-FESNF- 200 µM). Copper (b-0.25 equiv., c-0.5 equiv., d-1 equiv., and e-6 equiv.) was gradually added to the peptide solution. *Insert:* Differential absorption spectra in the presence of 1 or 6 equivalents of copper.

II.7.2. Spectrofluorimetric studies

The 3D fluorescence spectra were also analyzed at pH 5, 6, or 7 in 40 mM acetate buffer solution at 27 °C. The peptide itself (156 µM) exhibited two emission maxima at 213 and 283 nm (**Figure II.7.3** - A, C, D, and E). These bands are characteristic of phenylalanine residues (Bortolotti et al., 2016). In the presence of copper ions (10 equivalents), the emission intensity decreased in close dependence on the pH of the buffer solution used (**Figure II.7.3** - F, G, and H).

At a pH value of 5, only 36.5% of the initial fluorescence of the peptide was maintained when the excitation and emission wavelengths were chosen at their maxima of 258 and 283 nm. At pH values of 6 and 7, only 10.15% and 2.6% of the initial fluorescence was observed. In addition, the signal centered at 258/283 (ex/em) disappeared almost completely at pH 7 (**Figure II.7.3** - H), and the emission maximum at the excitation wavelength of 213 nm shifted to shorter wavelengths. At the same time, the emission maximum shifted to longer wavelengths (to a value of 310 nm). In addition, at pH 7, a signal with a maximum emission shifted approximately to the

spectral region 200/355 (ex/em) was observed, difficult to locate accurately due to the limitations of the instrument operating at excitation lengths greater than 200 nm.

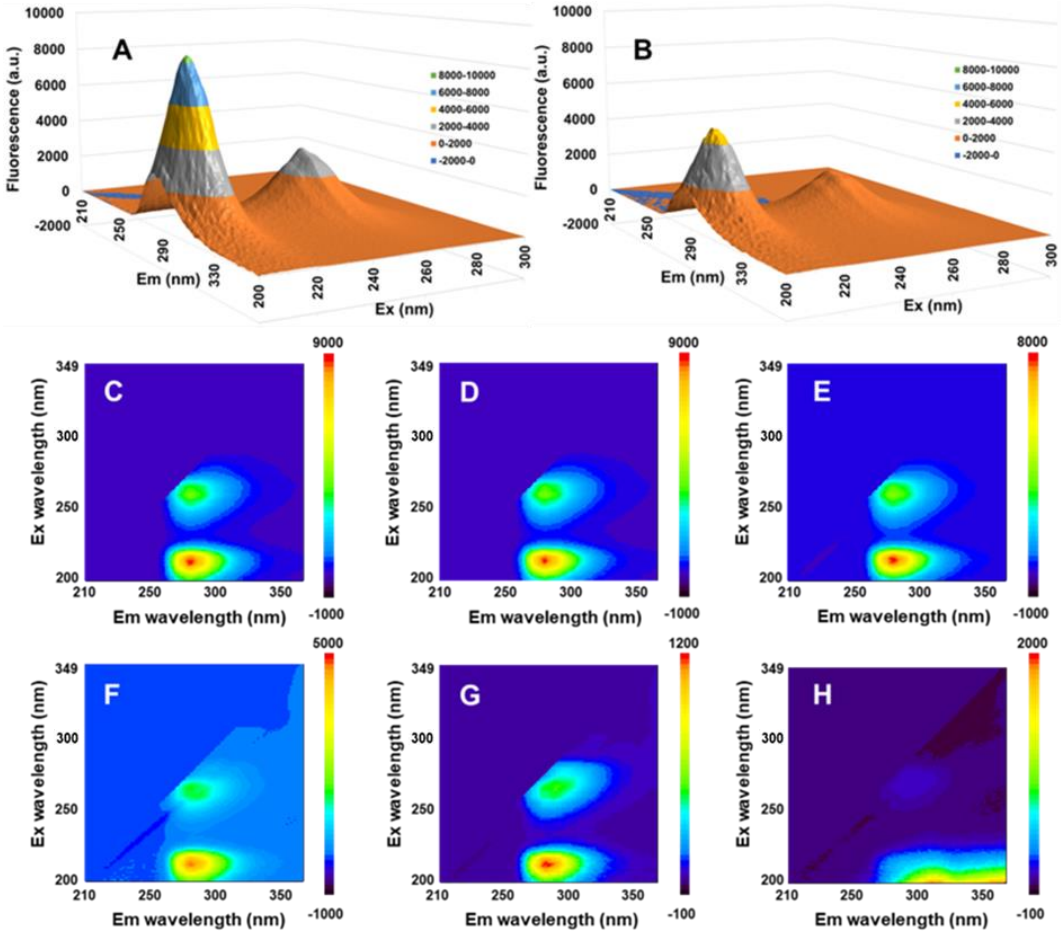

Figure II.7.3. 3D fluorescence spectra and contour maps of the free peptide or in the presence of Cu^{2+} ions. *Top row:* 3D spectra of the FESNF-NH_2 peptide (156 µM, A) and in the presence of 0.5 equivalents of copper (B) in 50 mM sodium acetate pH 7.0. *Middle row:* contour map for the pentapeptide analyzed at three different pH values (pH 5.0, 6.0, and 7.0 - C, D, and E). *Bottom row:* contour map for the pentapeptide in the presence of 10 equivalents of copper obtained at three different pH values (pH 5.0; 6.0 and 7.0 - F, G and H).

II.7.3. MALDI-ToF mass spectrometry analysis

The MALDI-ToF mass spectrum of the FESNF-NH_2 peptide, after incubating a 3 mM peptide solution with 30 µM Cu(II) ions for 20 hours at a physiological pH of 7.4 and a temperature of 37 °C, provides a detailed picture of the molecular species formed (**Figure II.7.4**). The monoprotonated molecular ion $[M+H]^+$ present at m/z 642.33, and the corresponding sodium adduct $[M+Na]^+$, at m/z 664.27, indicate the presence of unreacted peptide. The signals at m/z 704.25 and 726.25 correspond to the molecular ion of the peptide-Cu(II) complex, $[M+Cu(II)]^+$, and its Na adduct, $[M+Cu(II)+Na-H]^+$, respectively.

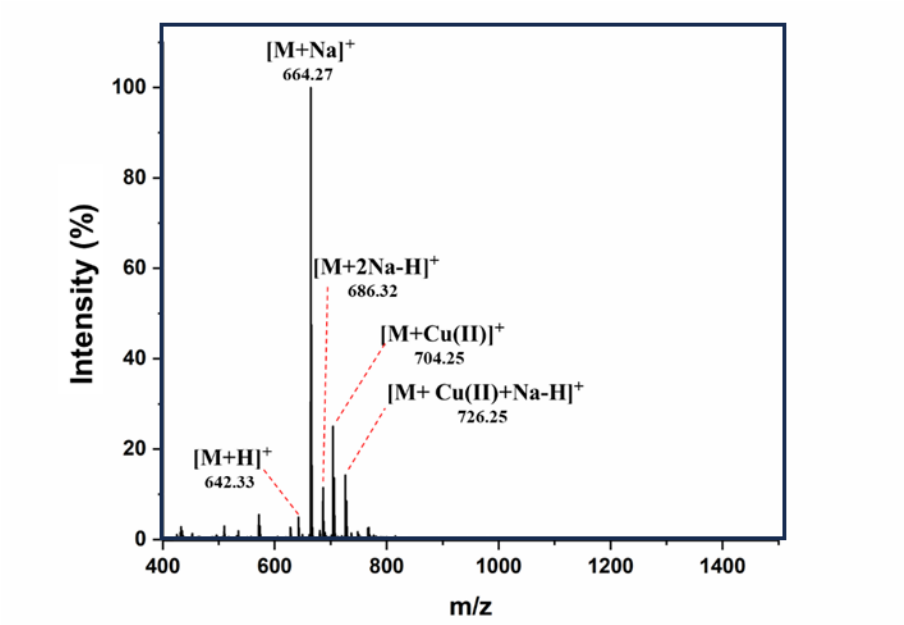

Figure II.7.4. MALDI-ToF mass spectrum of the FESNF-NH_2 peptide after complexation with Cu(II) ions. The DHB matrix was used.

III. MUTANT PEPTIDES WITH SELF-ASSEMBLY PROPERTIES

III.1. SELECTION OF MUTANT PEPTIDE SEQUENCES

Two mutant peptides were synthesized using solid-phase synthesis starting from the sequence of a previously obtained peptide whose self-assembly properties were investigated by UV-vis, spectrofluorimetric, *in silico*, and atomic force microscopy (AFM) studies at different pH values in **Chapter II**. Thus, a synthesis protocol identical to that applied to obtain the amide form of the FESNF-NH_2 sequence was followed, where the serine located in the central part of the pentapeptide was replaced with tyrosine in order to obtain the peptide with the sequence FEYNF-NH_2. Another mutant peptide was synthesized by replacing the phenylalanine at the C-terminal atom with tyrosine, resulting in the sequence FESNY-NH_2. Phenylalanine is a nonpolar amino acid, while tyrosine and serine are more polar amino acids due to the presence of a hydroxyl group in their structure. Serine has been studied in the context of amyloid fibril formation. For example, its role in the structure of amylin on the amyloid aggregation process has been found to be modest compared to that of 2-amino butyric acid in the structure of the corresponding mutant peptide (Akter et al., 2020). This supports the hypothesis that the hydrophobicity of amino acid units governs the aggregation mechanism.

Figure III.1.1 shows a comparison of the flat structures of the amide forms of the newly synthesized peptides (FEYNF, FESNY), the FESNF peptide described in **Chapter II**, and a peptide previously synthesized within the Biochemistry Group, with the sequence FEHNF.

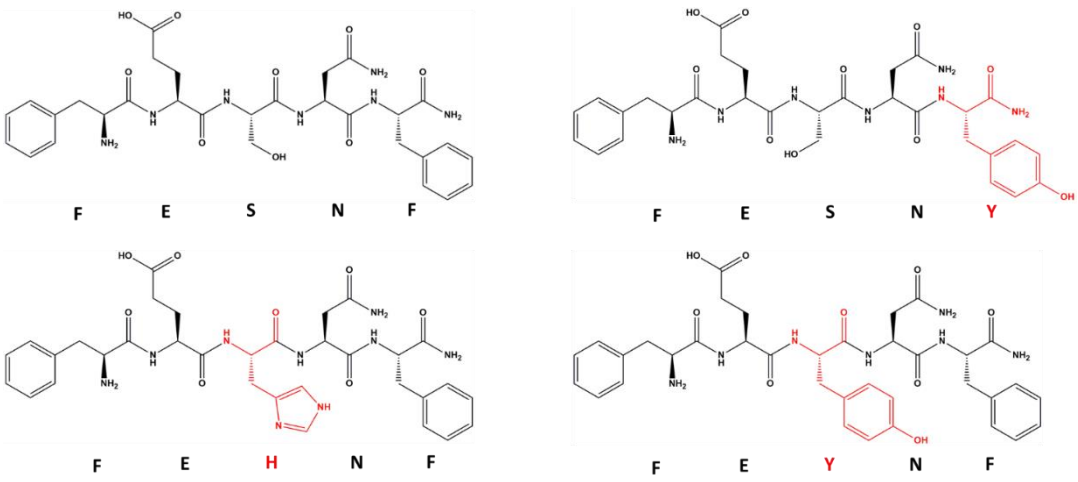

Figure III.1.1. Flat structures of the amide peptides FESNF, FEHNF, FEYNF, and FESNY created using ChemDraw Pro 12.0 software. In the case of mutant peptides, amino acids that differ from the reference peptide FESNF are highlighted in red.

III.3. MUTANT PEPTIDE FEYNF-NH_2

III.3.1. Qualitative analysis by RP-HPLC

Reverse-phase high-performance liquid chromatography (RP-HPLC) was used for the analysis and separation of the crude mixture of synthesized peptides. The HPLC profile of the FEYNF-NH_2 peptide is shown in **Figure III.3.1**. For specific detection of the peptide bond, the analysis was performed at a wavelength of 215 nm. The initial separation of the mixture followed a linear elution gradient, which allowed for clear fractionation and accurate identification of the compounds based on retention times.

In the first 5 minutes of the chromatogram, peaks corresponding mainly to acetic acid and possible residues of solvents used during synthesis were observed. However, a distinct peak appearing at 9.09 minutes was subsequently identified by mass spectrometry as the FEYNF-NH_2 peptide. The intensity of this signal clearly suggests that the purity of the peptide of interest exceeded 95%. A second peak, detected at 10.05 minutes, although weaker, corresponds to a more hydrophobic by-product with a slightly prolonged retention time, a phenomenon commonly encountered in solid-phase peptide synthesis (SPPS) (Guzmán et al., 2023). Mass spectrometry analysis of the secondary compound at the retention time of 10.05 min did not provide conclusive results, most likely due to the concentration being too low to be detected.

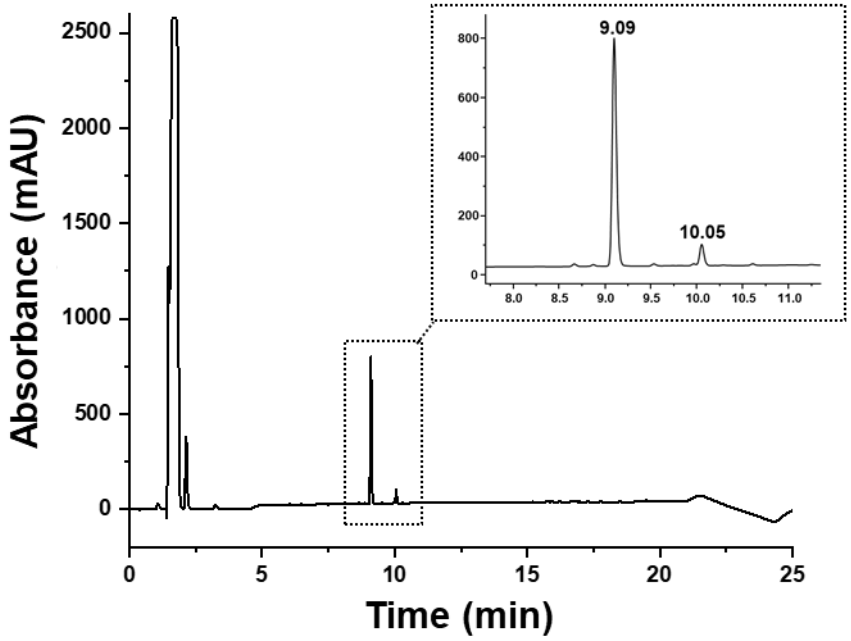

Figure III.3.1. HPLC chromatogram of crude FEYNF-NH_2 pentapeptide. The spectrum was recorded at a wavelength of 215 nm. Injection volume: 90 µL.

III.3.3. MALDI-ToF and MS/MS mass spectrometry analyses

Following mass spectrometry analysis of the first peak, the molecular ion $[M+H]^+$ of the pentapeptide was identified at m/z 718.40 with the DHB matrix (**Figure III.3.2** a) and slightly shifted to m/z 718.55 with HCCA (**Figure III.3.2** b). In addition to the protonated molecular ion, the presence of sodium adducts ($[M+Na]^+$) was also detected at m/z 740.41 and m/z 740.50, respectively, depending on the matrix used. The peptide tends to generate sodium adducts, possibly due to interactions between sodium ions and carbonyl oxygen and/or amide nitrogen. This interaction could be stabilized by the aromatic nucleus of the tyrosine side chain, a hypothesis previously supported in other studies (Moyer et al., 2003). Furthermore, potassium adducts ($[M+K]^+$) were also identified at m/z 756.51 and m/z 756.58, respectively.

Further analysis by collision-induced dissociation (CID) of the molecular ion [FEYNF + H]$^+$ (m/z 718.55) generated multiple b^+ and y^+ molecular fragments, providing valuable information about the fragmentation patterns of the FEYNF-NH_2 pentapeptide (**Figure III.3.2** c). The tandem mass spectrum highlights several distinct fragments, among which the abundance of signals corresponding to ionic fragments following ammonia elimination stands out: y^{2+}-NH_3 at m/z 261.87, y^{3+}-NH_3 at m/z 424.99, b^{4+}-NH_3 at m/z 537.99, and y^{4+}-NH_3 at m/z 553.61. Also, the loss of a water molecule can be correlated with the presence of the glutamic acid residue,

while the release of carbon dioxide could come from the decarboxylation of the same amino acid residue.

In the case of the signal at m/z 672.93 ($[M+H]^+$ - 46), the mass difference of 46 Da could reflect the simultaneous elimination of a CO_2 molecule and two H atoms. However, the elimination of a carbonyl group and a water molecule is much more likely, as it is unlikely that a hydrogen molecule would be eliminated from such peptides. Furthermore, detailed analysis of the MS/MS spectra shows that the uniform distribution of aromatic residues along the peptide chain favors fragmentation at all amide bonds. This behavior contrasts with that observed in the case of the mutant peptide FESNY-NH_2, where aromatic residues, located exclusively at the ends of the peptide chain, induce predominant fragmentation in the terminal regions (Jitaru et al., 2024). Previous studies have shown that the presence of residues with high electron density, such as phenylalanine and tyrosine, facilitates fragmentation in tandem mass spectrometry because it favors charge localization and increases the probability of molecule dissociation (Zhang, 2004).

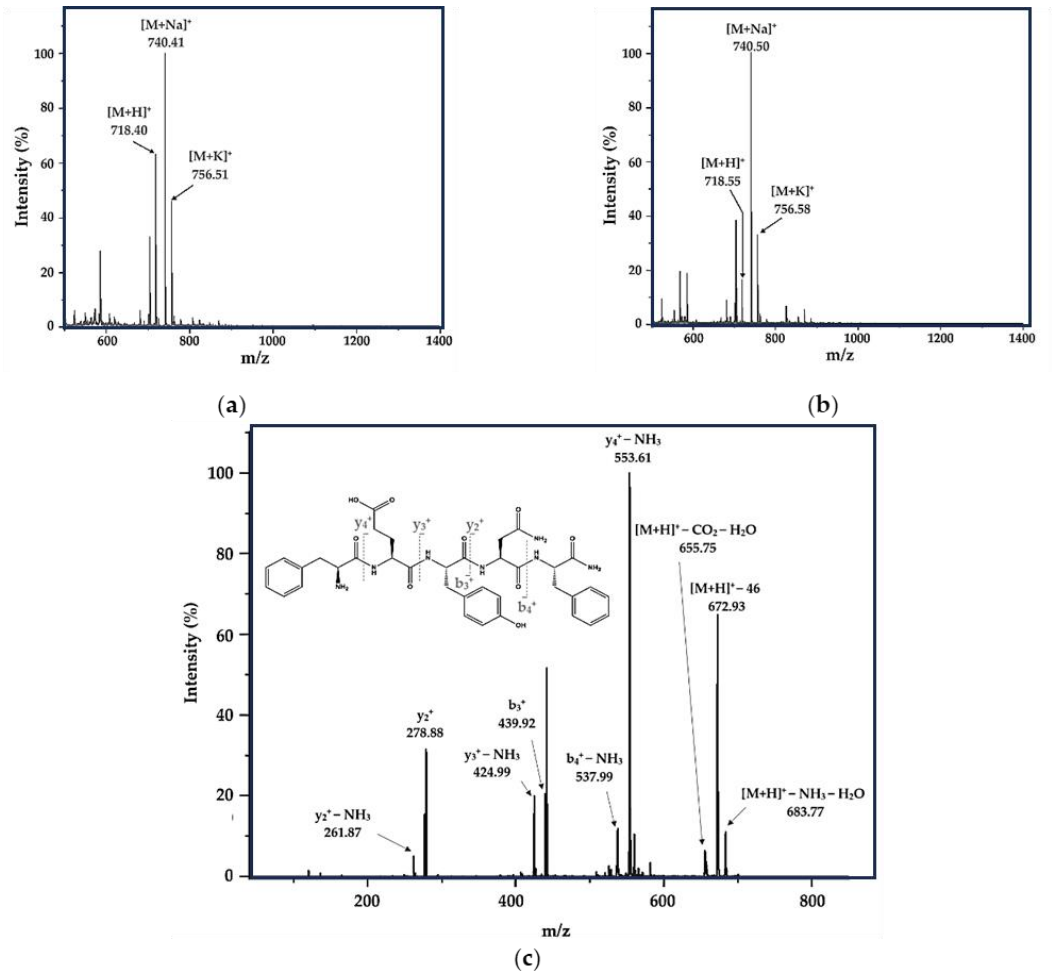

Figure III.3.2. MS spectrum of the fraction eluted at 9.09 min, confirming m/z corresponding to FEYNF-NH_2 with two different matrices: (a) DHB and (b) HCCA; (c) Assignment of m/z signals resulting from MALDI-ToF MS/MS tandem mass spectrometry analysis; fragmentation of the molecular ion $[FEYNF + H]^+$ (m/z 718.55) was performed by collision-induced dissociation (CID).

III.3.4. ESI-MS mass spectrometry analysis

The mass spectrum for the FEYNF-NH_2 peptide in **Figure III.3.3** confirms the existence of the peptide, which appears as a molecular ion $[M+H]^+$ at m/z 718.31. The mass spectrum also shows signals at m/z 1436.63, which were attributed to the dimer ion $[2M+H]^+$ and, possibly, to a doubly charged ion $[M+K+H]^{2+}$ at m/z 378.65. The binding of the potassium ion in the case of the $[M+K+H]^{2+}$ adduct most likely occurs at the carboxyl group in the side chain of glutamic acid (E) (Emmert et al., 2004).

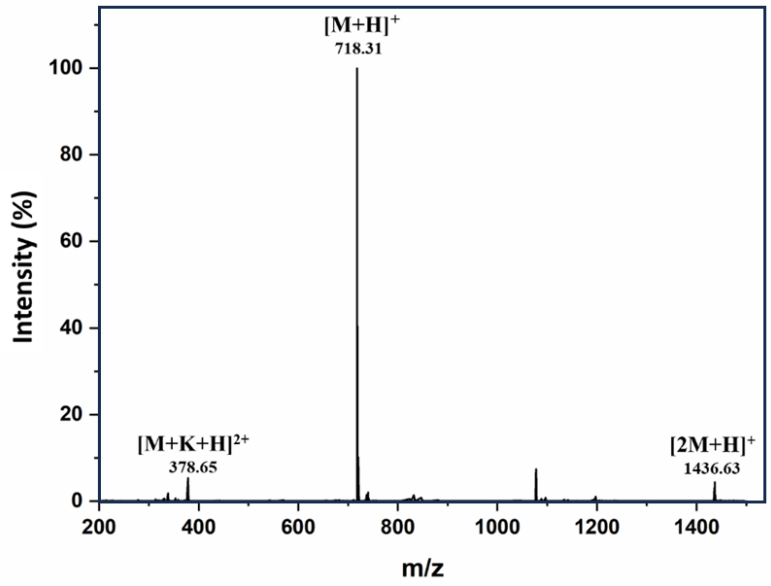

Figure III.3.3. ESI-MS mass spectrum of the FEYNF-NH_2 peptide.

III.3.5. Characterization of self-assembly properties

III.3.5.1. Fourier-transform infrared spectroscopy

The study of peptide self-assembly and its correlation with the secondary structure, in particular the formation of β-sheet structures, was carried out using Fourier Transform Infrared Spectroscopy (FTIR). To highlight the secondary structure of the FEYNF-NH_2 peptide, the analysis focused mainly on the amide I bands.

The secondary structure of the FEYNF-NH_2 peptide was analyzed by quantitative deconvolution of the FTIR bands, using Gaussian fitting functions (**Figure III.3.5**). Data processing was performed with the OriginPro 8.5.0 SR1 software (OriginLab Corporation, Northampton, MA, USA). The corresponding structures were identified based on literature data, as illustrated in **Figure III.3.5** (Bagińska et al., 2008; Barreto et al., 2020; De Meutter and Goormaghtigh, 2021; Seo et al., 2016).

It can be observed that the most significant absorption bands are located at 1633 cm^{-1} and 1672 cm^{-1}, corresponding to β-sheet and β-turn structures, respectively. This finding is supported

by the data presented in **Table III.3.3**, which show that the peaks associated with β-sheet and β-turn structures contribute significantly to the overall area of the amide I bands. Although the self-assembly of the FEYNF-NH_2 peptide is dominated by β-sheet structures, the FTIR spectrum also reveals signals associated with α-helical structures as well as features characteristic of side chain groups or bonds. Nevertheless, according to the FTIR analysis, the main structural pattern observed in the peptide self-assembly can be attributed to the formation of β-sheet structures. Consequently, the following subsections present the results of additional analyses performed to gain a deeper understanding of the specific features of FEYNF-NH_2 peptide self-assembly.

Table III.3.3. Secondary structure composition (%) of the FEYNF-NH_2 peptide determined by FTIR spectral analysis.

Peak no.	Structure	Wavenumber (cm^{-1})	Relative intensity (%)*
1	Antiparallel β-sheet	1694	3.12
2	β-turns	1672	16.12
3	α-helix	1657	28.01
4	β-sheet	1633	34.53
5	β-sheet aggregate strands	1613	10.56
6	Side chain	1596	7.65

*Relative intensity indicates the proportion of a specific component band in relation to the total area of the amide region I.

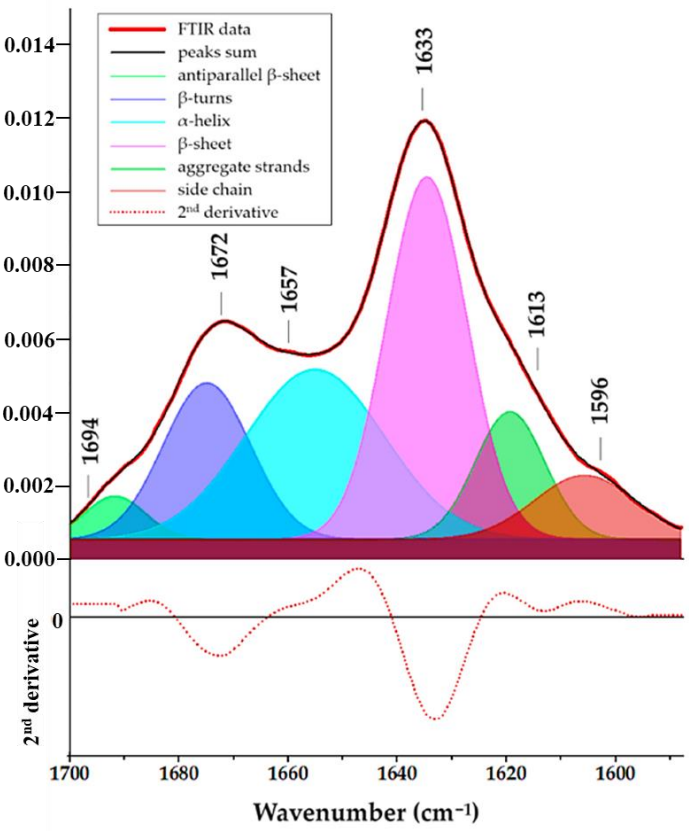

Figure III.3.5. FTIR spectrum corresponding to the amide I region, highlighting the secondary structures of the FEYNF-NH_2 peptide in the solid state, obtained by Gaussian deconvolution based on the second derivative spectrum of the original data.

III.3.5.3. Transmission electron microscopy analysis

Peptide subunits can form a range of complex non-covalent interactions both in the solid state and in solution, which promotes the self-assembly process into well-organized structures. These supramolecular architectures can further evolve through additional self-assembly processes, leading to the formation of a variety of nano- and microstructures with potential applications in the development of materials with functional properties (Konda et al., 2016).

Therefore, to evaluate the morphological characteristics of the newly synthesized FEYNF-NH_2 peptide, transmission electron microscopy (TEM) was employed (**Figure III.3.7** a,b). In addition, energy-dispersive X-ray spectroscopy (EDX) integrated into the TEM system confirmed the elemental composition and purity of the synthesized peptide through the presence of characteristic C, N, and O elements (**Figure III.3.7** b,c). It is worth noting that the variations in carbon signal intensity are mainly due to the use of carbon grids for TEM analysis.

TEM images of the pentapeptide, previously dispersed in a phosphate buffer and dimethyl sulfoxide (DMSO) solution, are shown in **Figure III.3.7** a. The formation of extended nanotape structures with overlapping regions, resulting from peptide self-assembly, can be observed. This phenomenon could be attributed to the increased density of transient non-covalent

interactions between the self-assembled nanostructures (Gelain et al., 2020). Moreover, this planar and extended organization is characteristic of β-sheet structures.

Considering the potential biomedical applications, the peptide was subjected to controlled incubation under physiological conditions (37 °C for 20 hours). The TEM image of the dehydrated peptide is shown in **Figure III.3.7** b. Compared to **Figure III.3.7** a, it was observed that following incubation, the FEYNF peptide tends to form fibrillar structures as well as some supramolecular tape-like organizations.

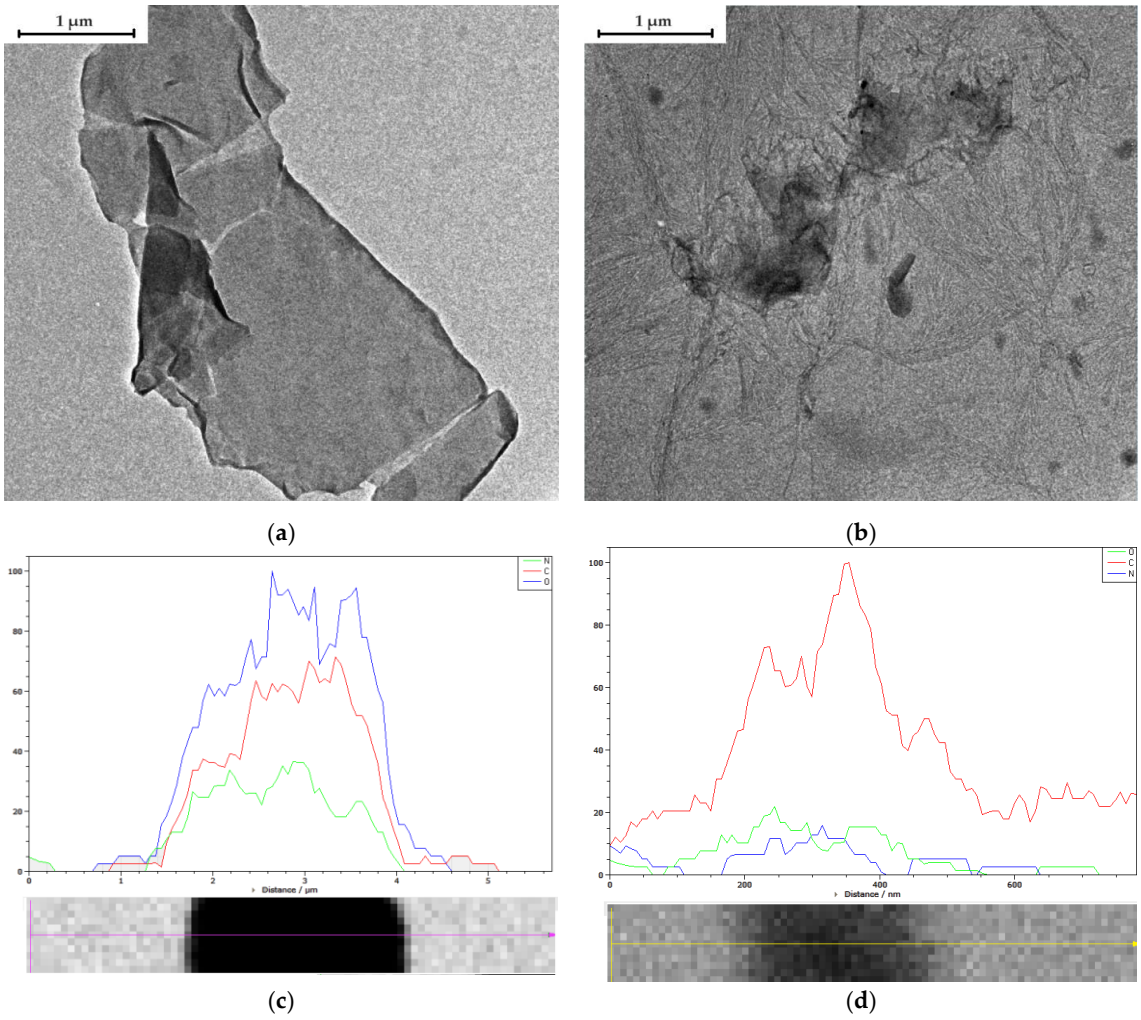

Figure III.3.7. TEM images of FEYNF-NH_2 before (a) and after 20 hours of incubation under physiological conditions (pH 7.4, 37 °C) (b); EDX spectra for the FEYNF peptide sample before (c) and after incubation (d).

III.3.5.4. Polarized light microscopy analysis

A defining factor determining the physical and chemical properties of self-assembling peptides (and amino acids) is molecular orientation (Zhou et al., 2022). Optical analysis based on polarization has proven to be extremely useful in molecular studies, especially when it comes to molecular orientation. **Figure III.3.8** shows images obtained at two different polarization angles (0° and 90°), as well as at two different magnifications. It can be observed that the FEYNF

peptide self-assembles into a complex, highly branched architecture characterized by extensive dendritic patterns. In **Figure III.3.8** c, the short branches oriented nearly perpendicular to the nanofiber axis are more clearly visible. This type of organization has also been reported by other researchers, who noted the presence of "entangled" fibrils formed during gelation, a feature typical of supramolecular hydrogels (Chakraborty et al., 2020).

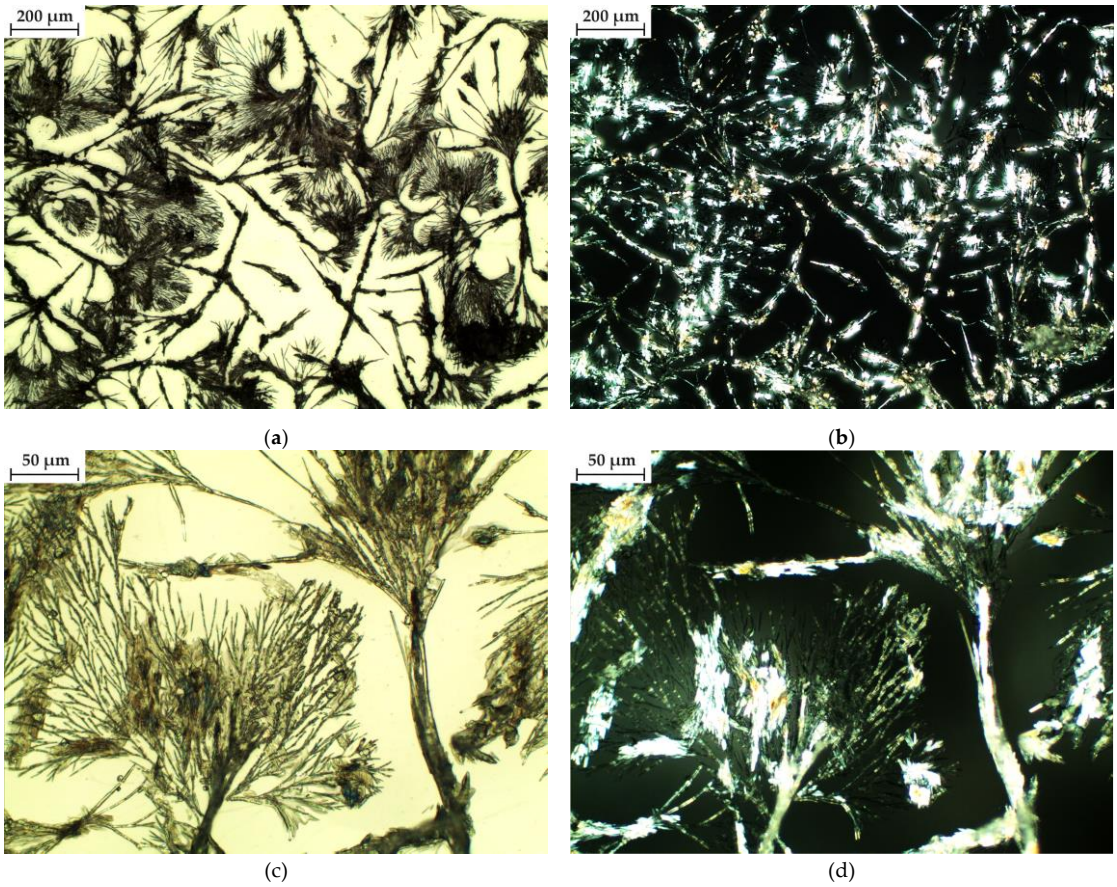

Figure III.3.8. Microscopic images of dehydrated samples from FEYNF-NH_2 (3 mM) solutions incubated under physiological conditions (pH 7.4, 37 °C), recorded at two polarization angles: 0° (a, c) and 90° (b, d) and at different magnification scales.

The morphology of FEYNF can be primarily attributed to the presence of the tyrosine residue. It is well known that, at physiological pH 7.4, the tyrosine residue remains predominantly neutral, promoting interactions that favor the initiation of fibrillogenesis (DiCostanzo et al., 2012). Compared to the previously studied peptide (FESNF-NH_2) analyzed under similar pH conditions (Jitaru et al., 2023), the introduction of tyrosine appears to be the main factor driving the observed morphological differences. This structural modification can be mainly explained by the presence of the aromatic ring and hydroxyl group in tyrosine. In addition to the role of phenylalanine residues, recognized for promoting π–π and hydrophobic interactions, tyrosine can significantly influence the peptide self-assembly process. A notable aspect is that the theoretically calculated isoelectric point for the FEYNF peptide (6.94) is very

close to that of the FESNF peptide (6.99). Furthermore, FEYNF-NH_2 exhibits fibril-forming characteristics similar to those of β-amyloid (Aβ) peptides near its isoelectric point (Tian and Viles, 2022).

Figures III.3.8 b,d, recorded at a polarization angle of 90°, confirm that the self-assembled species derived from the FEYNF-NH_2 peptide exhibit birefringence under polarized light. This indicates the presence of β-sheet structures within the self-assembled architecture, leading to the formation of well-organized crystalline structures. Other studies have shown that temperature can affect the way peptides self-assemble, resulting in the formation of well-aligned peptide nanofiber bundles that can create birefringent regions visible to the naked eye, with sizes on the order of tens of millimeters (Accardo and Handelman, 2022; S. Zhang et al., 2010).

III.3.6. *In silico* studies

III.3.6.2. Study of β-sheet structure formation

In the conformation shown in **Figure III.3.11**, the FEYNF-NH_2 peptide demonstrates the ability to adopt a β-sheet structure, a phenomenon that facilitates the extension of β-strands as oligomer growth occurs, thereby indicating a tendency to form fibrils.

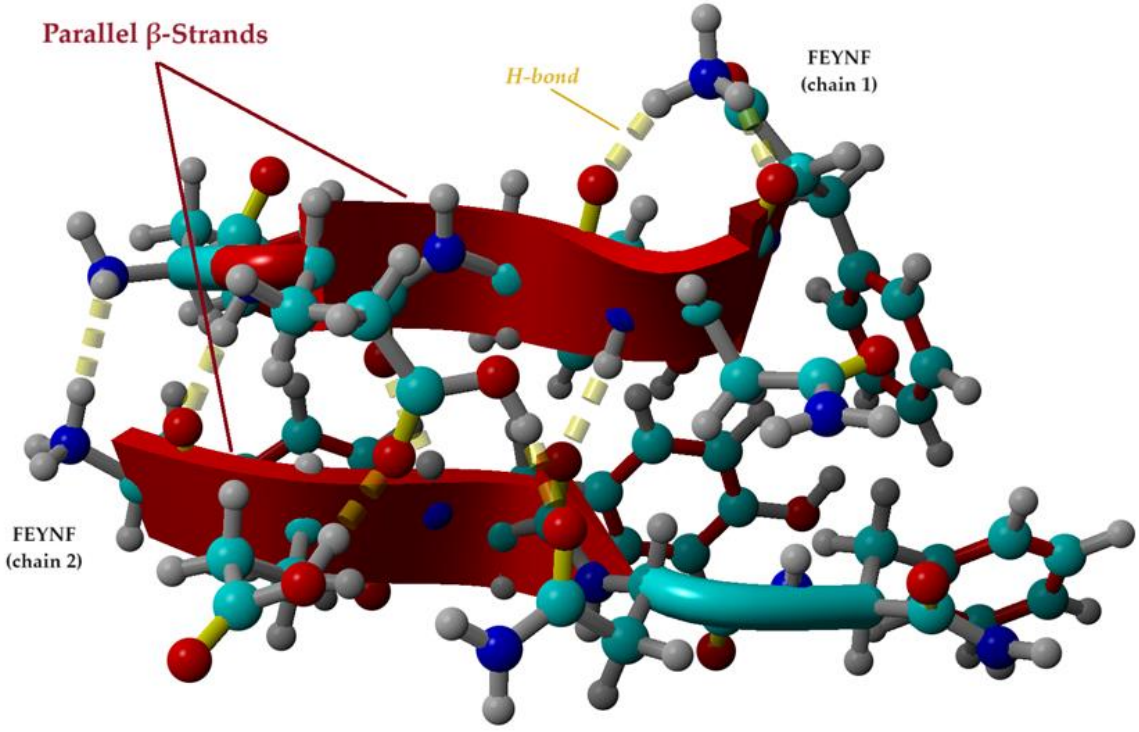

Figure III.3.11. Optimized conformation of the protonated dimer (FEYNF@FEYNF(+2)), calculated using the YASARA force field, suggesting the self-assembly and gelation mechanism of the FEYNF peptide into a β-sheet structure. Atom color code: cyan – carbon, blue – nitrogen, red – oxygen, gray – hydrogen.

III.3.6.3. Potential implications in polyplex formation

Peptide-based non-viral vectors are considered ideal candidates for gene therapy, primarily due to their ability to traverse cellular membranes (Yang and Luo, 2023). In this context, the potential of the FEYNF peptide to form polyplexes was investigated through *in silico* studies, using molecular docking simulations.

Thus, the protonated dimer FEYNF@FEYNF, shown in **Figure III.3.11**, was used in a second molecular docking study, with an oligonucleotide DNA sequence as the receptor. For this purpose, the Drew–Dickerson dodecamer d(CGCGAATTCGCG)$_2$ was used as a model to simulate a short DNA helix (Cojocaru et al., 2021)

The optimal docking pose between the protonated dimeric complex (FEYNF@FEYNF(+2)) and the oligonucleotide DNA sequence (DDD(−25)) is shown in **Figure III.3.15**. This configuration is the most favorable in terms of the lowest binding energy ($E_{(b)}$ = −12.49 kcal/mol). Moreover, the extremely low dissociation constant (K_d= 0.694 nM), at the nanomolar scale, characteristic of a stable complex, confirms the formation of the polyplex of interest. As shown in **Figure III.3.15**, polyplex formation is governed by non-covalent interactions, including hydrophobic interactions, inter- and intramolecular hydrogen bonds, π–π interactions, and cation–π interactions.

The FEYNF peptide forms supramolecular assemblies capable of compacting nucleic acids, converting B-form DNA into a denser structure characteristic of polyplexes. This process is essential in gene therapy. DNA compaction serves a dual purpose: it provides protection against premature degradation and facilitates cellular membrane crossing, particularly via mechanisms such as endocytosis, resulting in more efficient cellular uptake.

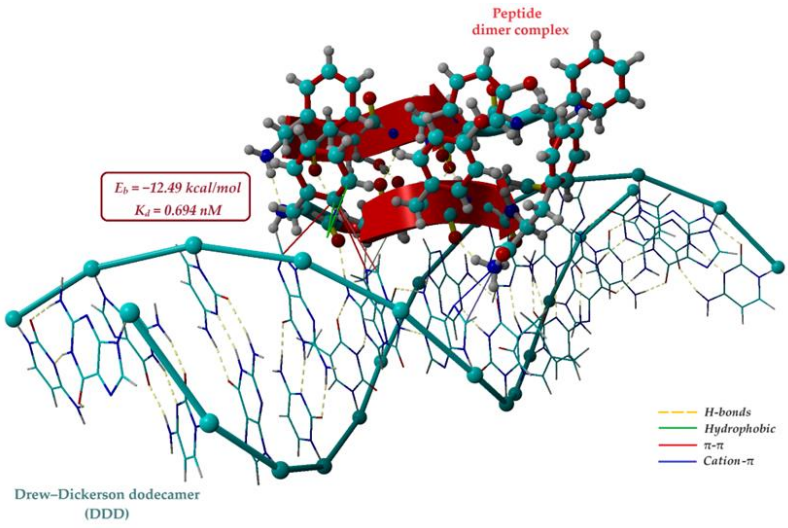

Figure III.3.15. Optimal polyplex conformation obtained from molecular docking simulation, showing the non-covalent interactions between the protonated dimer (FEYNF@FEYNF) as the ligand and the Drew–Dickerson dodecamer d(CGCGAATTCGCG)$_2$ as the receptor.

III.4. MUTANT PEPTIDE FESNY-NH_2

III.4.1. Qualitative analysis by RP-HPLC

In **Figure III.4.1** a, two main signals can be observed at 7.05 and 8.25 minutes, resulting from the chromatographic separation of the crude peptide with the sequence FESNY-NH_2, obtained after the synthesis, precipitation, and redissolution steps. The presence of a limited number of signals in the raw mixture after elution indicates a relatively pure target compound. These signals were further analyzed by mass spectrometry. The intense signals at the beginning of the chromatogram are most likely due to the presence of glacial acetic acid and an overlap from the signal generated by the sample injection into the system.

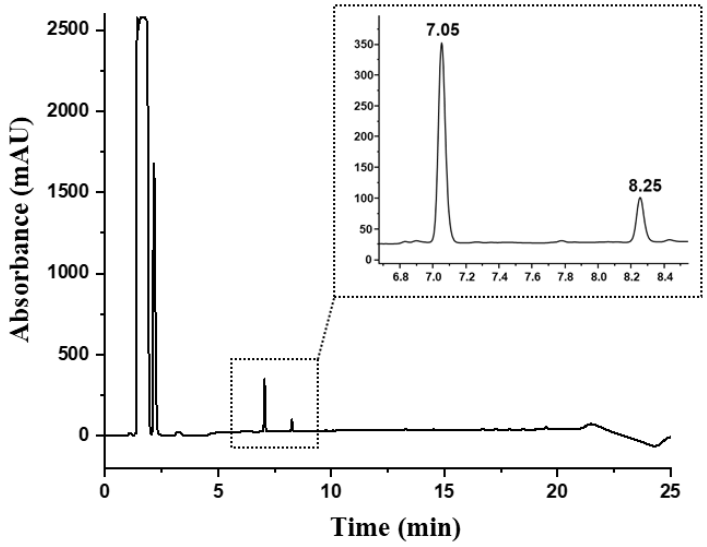

Figure III.4.1. HPLC chromatogram of one of the fractions obtained after redissolution in 5% acetic acid for the FESNY sequence. The spectrum was recorded at 215 nm. Injected volume: 150 µL.

III.4.2. MALDI-ToF and MS/MS mass spectrometry analyses

The mass spectra shown in **Figure III.4.2** confirm the structure of the peptide of interest at the retention time of 7.05 min, using both DHB and HCCA matrices. The MS spectrum indicated a mass-to-charge ratio (m/z) of 658.32, corresponding to the molecular ion $[M+H]^+$. In addition, sodium ($[M+Na]^+$) and potassium ($[M+K]^+$) adducts were observed at m/z 680.28 and m/z 696.28, respectively. Comparing the mass spectrum of the target compound in **Figure III.4.2** B with the reference spectrum of the HCCA matrix reveals intense signals attributed to the matrix rather than the analyte. Furthermore, the by-product eluting at 8.25 min could not be identified by mass spectrometry because the collected analyte sample was too dilute.

The tandem mass spectrum (MS/MS) obtained by collision-induced dissociation (CID) of the molecular ion of interest $[FESNY + H]^+$ (m/z 658.32) in the mass spectrometer is shown

in **Figure III.4.3**. These fragments underwent various processes such as dehydration, deamination, or decarboxylation, leading to the appearance of signals at the corresponding m/z values. Specifically, m/z 416.12 corresponds to the b_4^+ fragment with the loss of a water (H_2O) molecule and a carbon dioxide (CO_2) molecule; m/z 460.02 represents the b_4^+ fragment with the loss of a water molecule (H_2O); and m/z 476.18 corresponds to the y_4^+ fragment with the loss of a water molecule (H_2O) and an ammonia molecule (NH_3). Additionally, at m/z 598.26 ($[M+H]^+ - 60$), the 60 Da difference could correspond to the loss of a CO_2 molecule and an oxygen atom or an $–NH_2$ group. Similarly, at m/z 642.14 ($[M+H]^+ - 16$), the neutral loss of 16 Da could correspond to the elimination of an $–NH_2$ group.

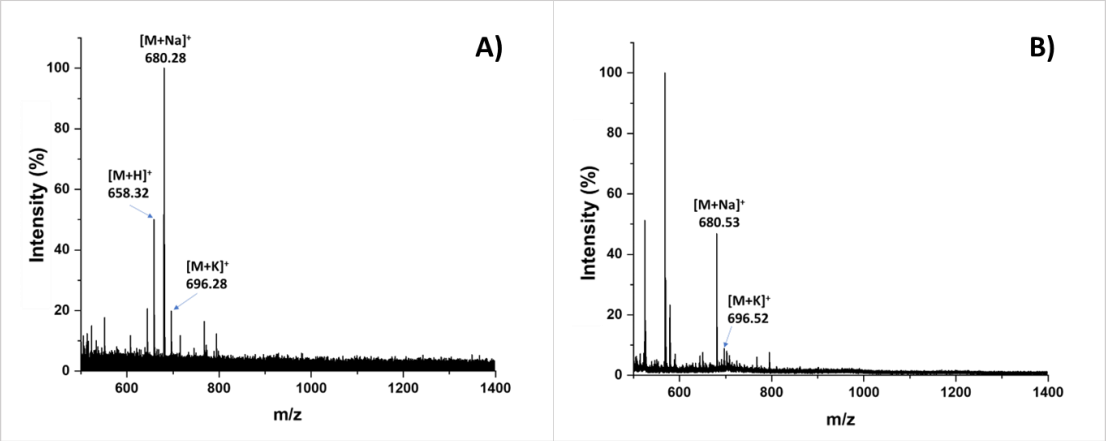

Figure III.4.2. MS spectrum of the fraction eluted at 7.05 min confirming the m/z corresponding to FESNY using two different matrices: A) DHB; B) HCCA.

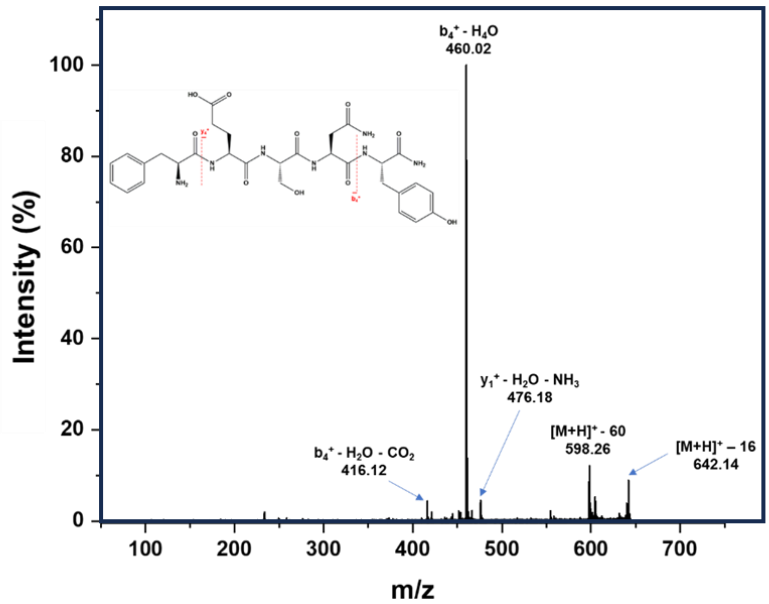

Figure III.4.3. Assignment of m/z signals resulting from MALDI-ToF MS/MS analysis. Fragmentation of the molecular ion $[FESNY + H]^+$ (m/z 658.32) was performed by collision-induced dissociation (CID) for the fraction collected at 7.05 min.

Moreover, the spectra obtained from tandem mass spectrometry analysis (**Figure III.4.3**) suggested that the peptide is more prone to fragment at the termini, where the aromatic residues are located, rather than in the central region of the peptide chain. The presence of phenylalanine and tyrosine residues, due to their relatively high electron density, particularly in the aromatic rings, can facilitate fragmentation by promoting charge localization and increasing susceptibility to dissociation processes in tandem mass spectra (Zhang, 2004).

III.4.3. ESI-MS mass spectrometry analysis

The mass spectrum shown in **Figure III.4.4** indicates three main signals: the protonated molecular ion $[M+H]^+$ at m/z 658.28, a sodium adduct $[M+Na]^+$ at m/z 680.26, and a doubly protonated ion $[M+K+H]^{2+}$ at m/z 348.38. Furthermore, it is noteworthy that the FESNY peptide, which contains an acidic residue at position 2 of the sequence, is prone to forming multiple adducts with alkali metal ions, both as ionization agents and as substitutes for acidic protons. In this context, the formation of the $[M+K+H]^{2+}$ ion is a relevant example of this tendency, where potassium participates alongside a proton in the peptide's double charge (Emmert et al., 2004).

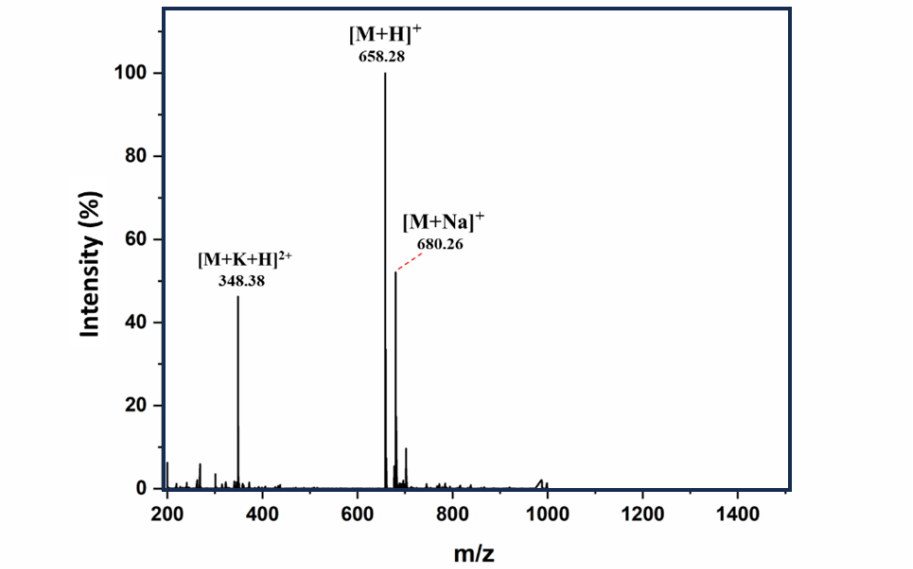

Figure III.4.4. ESI-MS spectrum of the FESNY-NH_2 peptide.

III.4.5. Polarized light microscopy analysis

Images obtained by polarized light microscopy show that the FESNY-NH_2 peptide self-assembles under physiological conditions into highly branched structures characterized by extensive dendritic patterns (**Figure III.4.7**) (Tomalia, 2024). The amidated C-terminus of the peptide may contribute to reducing the overall charge, which could lead to decreased solubility. On the other hand, this modification may enhance peptide stability, making it more similar to

native proteins present in the body. These considerations could amplify the biological significance of the peptide's activity (Arispe et al., 2008).

The theoretical isoelectric point of the FESNY-NH_2 peptide is 6.94 (Peptide Bachem Calculator). Under physiological conditions (pH 7.4), the tyrosine residue most likely remains in a neutral state. This neutrality allows tyrosine to mediate the interactions necessary for initiating fiber formation (DiCostanzo et al., 2012). Compared to the previously studied peptide (FESNF-NH_2) under the same pH conditions, the presence of tyrosine at the C-terminal end in the FESNY-NH_2 sequence differs very little from the native peptide. The structural modification is mainly due to the hydroxyl group located at position 4 on the aromatic ring.

It is important to note that the theoretical isoelectric points of the two peptides, FESNF and FESNY, are very close (6.99 and 6.94, respectively). Nevertheless, the behavior of the FESNY-NH_2 peptide appears to resemble that of β-amyloid (Aβ) peptides in terms of fibril formation, particularly under pH conditions close to their isoelectric points (Tian and Viles, 2022).

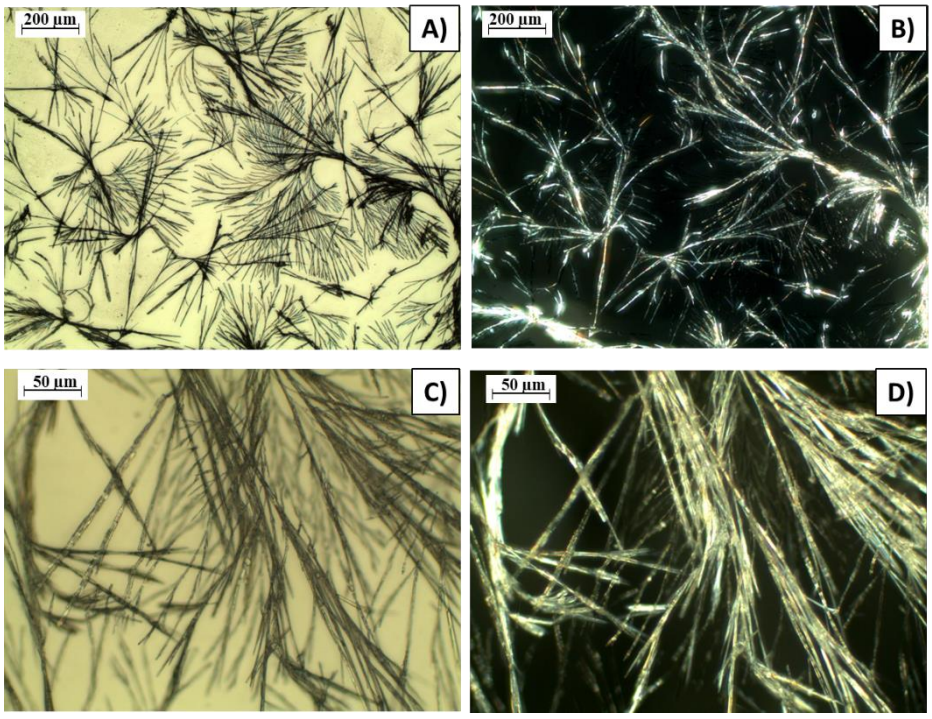

Figure III.4.7. Microscopic images of dehydrated samples from FESNY-NH_2 solutions incubated at physiological pH 7.4 and 37 °C, captured under two polarization angles: a) 0° (A, C) and b) 90° (B, D). Scale: i) 200 µm (A, B); ii) 50 µm (C, D).

III.5. MUTANT PEPTIDE FEHNF-NH_2

III.5.1. ESI-MS mass spectrometry analysis

For the characterization of the FEHNF-NH_2 peptide, previously synthesized in the Biochemistry Group, ESI-MS was used. In the mass spectrum (**Figure III.5.1**), signals

corresponding to the mono- and doubly charged molecular ions, $[M+H]^+$ and $[M+2H]^{2+}$, can be observed at m/z 692.31 and m/z 346.66, respectively, in agreement with the theoretical values. Additionally, the presence of the $[M+2H–NH_3]^{2+}$ ion at m/z 338.34 suggests the loss of an ammonia molecule, a phenomenon often observed under mild ionization conditions.

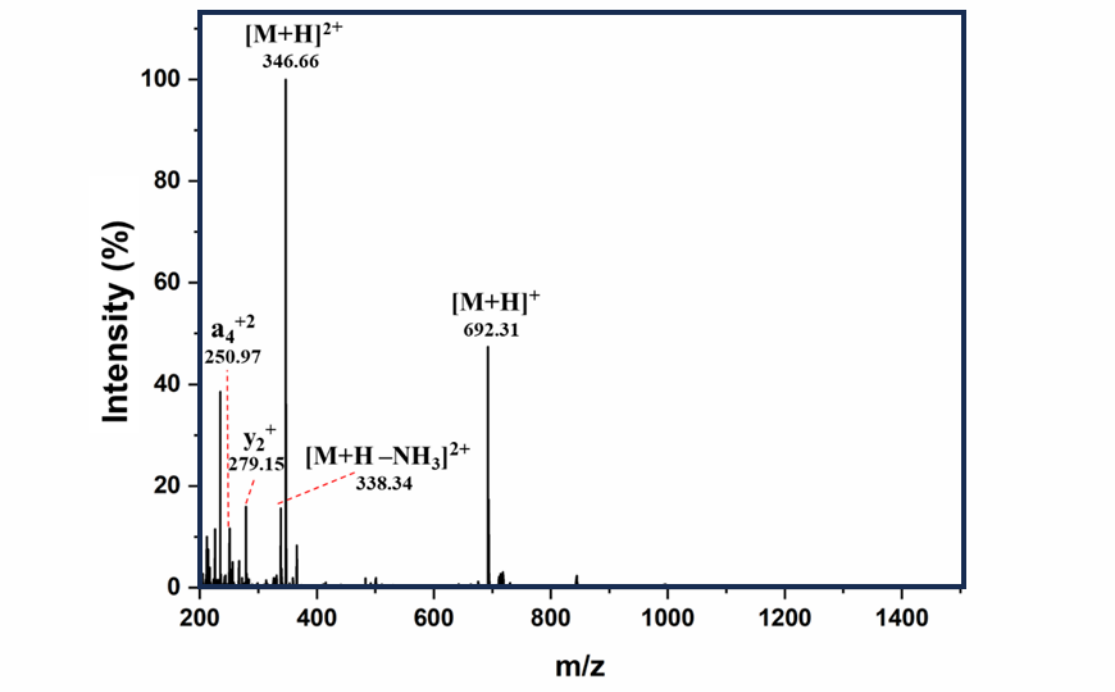

Figure III.5.1. ESI-MS spectrum of the FEHNF-NH_2 peptide.

III.5.2. Polarized light microscopy analysis

Compared to the fibrillar structures observed for the FESNF, FEYNF, and FESNY peptides, images obtained for the mutant FEHNF peptide using polarized light microscopy after incubation at 37 °C and pH 7.4 indicated the formation of spherical microstructures with radial projections.

The presence of histidine (H) in the FEHNF sequence, compared to serine (S) or tyrosine (Y) at position three in the previously studied mutant, was important for understanding the self-assembly mechanism. Histidine is an amino acid with an imidazole side chain that can be protonated or deprotonated depending on the pH of the environment. At pH 7.4, which is close to the pKa of the histidine imidazole group (approximately 6.0), a significant proportion of histidine residues will be neutral, but some may still be protonated, carrying a positive charge (Chen et al., 2022). The amphoteric property of histidine can critically influence intermolecular interactions and, consequently, the self-assembly process.

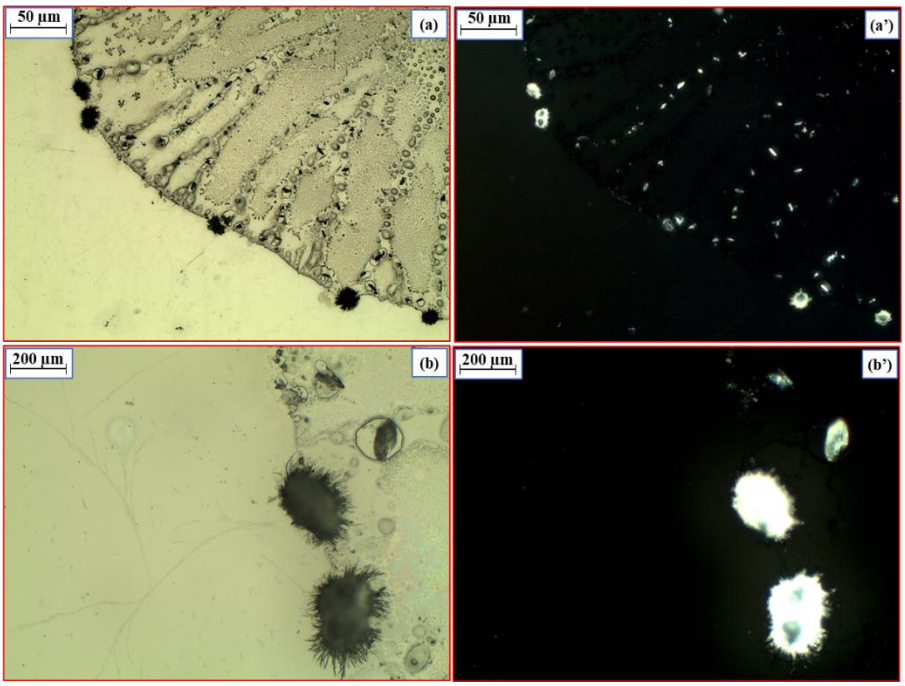

Figure III.5.2. Microscopic images of dehydrated samples from FEHNF-NH_2 peptide solutions incubated at physiological pH 7.4 and 37 °C, captured under two polarization angles: a) 0° (a, b) and b) 90° (a', b'). Scale: i) 200 µm (a, a'); ii) 50 µm (b, b').

GENERAL CONCLUSIONS

This doctoral thesis, entitled "*Short Peptides with Self-Assembly Properties: Synthesis, Characterization, and Potential Applications*", focused on elucidating the self-assembly mechanisms of small peptides containing aromatic residues. Thus, a comprehensive approach was adopted, correlating data from the current literature with our own experimental observations, while providing novel insights into this process.

The theoretical part of the thesis focused on analyzing the current scientific literature regarding the self-assembly properties of short peptides. Regarding the personal contributions, the doctoral research followed the initially proposed research directions, and all formulated objectives were fully achieved. Based on the obtained results, the following conclusions can be drawn:

O1. *Synthesis of a naturally occurring peptide sequence for the study of self-assembly*

Starting from the primary structure of lysozyme present in hen egg white, a peptide sequence with self-assembly potential, FESNF, was selected. This sequence was subsequently obtained via solid-phase peptide synthesis (SPPS), using the Fmoc/tBu strategy. The use of a Rink amide solid support allowed the production of a C-terminally amidated peptide, consistent with the native form of many endogenous peptides. This approach ensured compatibility with natural biological systems and reduced electrostatic repulsions that could hinder the self-assembly process in subsequent studies.

O2. *Synthesis of tyrosine analogs to analyze their impact on the self-assembly process*

Two mutant peptides, FEYNF-NH_2 and FESNY-NH_2, derived from the native peptide FESNF-NH_2, were selected for this study. In the first variant, phenylalanine was replaced with tyrosine, considering the structural similarity between the two amino acids. Both are aromatic and can participate in hydrophobic and π–π interactions, playing a crucial role in the formation of self-assembled structures. In addition, the hydroxyl group specific to tyrosine provides additional potential for hydrogen bonding, which can influence the stability of these structures. On the other hand, the replacement of serine with tyrosine aimed to introduce an aromatic moiety into an initially polar region lacking such groups, in order to evaluate its effect on the self-organization capacity. Both mutant peptides were synthesized via SPPS, featuring C-terminal amidation.

O3. *Optimization of peptide purification and separation by RP-HPLC and RP-SPE*

The RP-HPLC chromatograms of the crude mixtures of newly synthesized peptides revealed the presence of secondary compounds in each of the three syntheses. These by-products were more hydrophobic than the target peptides, eluting at longer retention times. The separation of the analytes was achieved with good resolution, allowing the individual collection of each chromatographic peak and their subsequent analysis by mass spectrometry. For the FEYNF and FESNY peptides, a reversed-phase solid-phase extraction (RP-SPE) protocol, adapted from the literature, was applied. Optimization of the purification method involved adjusting the pH of the eluted fractions with glacial

acetic acid solutions to a working pH of 4.5, compatible with the technical specifications of the stationary phase. This adjustment facilitated the elimination of an additional lyophilization step.

O4. *Peptide analysis by mass spectrometry for the confirmation of molecular masses, structures, and purity*

For the comprehensive characterization of the synthesized peptides, advanced complementary analytical techniques were employed, including MALDI-ToF MS, tandem mass spectrometry, and ESI-MS. The analysis of the FESNF peptide by MALDI-ToF and ESI-MS confirmed its molecular mass and, importantly, its structure, supported by the presence of characteristic MS/MS fragments. In addition, an N-alkylated by-product was characterized, showing a mass excess of 106 Da, which resulted from incomplete cleavage of the peptide from the resin. The other synthesized peptides, FEYNF-NH_2 and FESNY-NH_2, were successfully characterized, with both their molecular masses and fragmentation patterns being identified. FEYNF-NH_2 exhibited a tendency to form adducts and dimers, whereas FESNY-NH_2 was distinguished by preferential fragmentation at its termini. Furthermore, the FEHNF peptide, synthesized previously within the Biochemistry Group and used in preliminary self-assembly studies, was analyzed by ESI-MS, displaying characteristic m/z signals of its structure, along with a high susceptibility to fragmentation, confirmed by the presence of y_2^{2+} and a_4^{2+} ions.

O5. *Characterization of the FESNF peptide by UV-Vis spectroscopy, spectrofluorimetry, aggregation capacity, and complex formation with Cu(II) ions*

The FESNF-NH_2 peptide was characterized spectroscopically by UV-Vis and spectrofluorimetry, showing the specific absorption of phenylalanine at 258 nm and amide bonds at 203 nm. The fluorescence intensity at 282 nm, which varied proportionally with sample concentration, indicated the maintenance of a stable colloidal state within the concentration range of 25–250 µg/mL. Aggregation capacity was assessed through the aggregation index, which showed a tendency to increase under mildly acidic conditions, and by the ThT assay, which suggested the formation of small, ordered structures that are difficult to detect spectroscopically. Binding of Cu^{2+} ions to the FESNF peptide was evidenced by UV-Vis, spectrofluorimetric, and MALDI-ToF mass spectrometric studies. At pH 6.5, an increase in absorbance was observed, while at pH 7 fluorescence quenching occurred, suggesting the formation of a peptide–metal complex. Mass spectrometry analysis confirmed the presence of the FESNF–Cu(II) complex, while polarized light microscopy indicated that Cu^{2+} ions promote the self-assembly into more organized structures compared to the peptide alone.

O6. *Analysis of peptide self-assembled structures by AFM, TEM, and/or POM microscopy*

AFM images of FESNF peptide aggregates revealed a clear pH-dependent self-assembly behavior, consistent with spectroscopic data. Depending on the pH of the TRIS buffer solution, the structural assemblies displayed distinct morphologies: at pH 7.4, porous clusters were observed,

whereas at pH 8.2 compact nanofibrils were formed. TEM and POM studies showed that the peptides FEYNF-NH_2 and FESNY-NH_2 exhibited strong self-assembly tendencies under physiological pH, forming fibrillar nanostructures with extensive branching. The presence of tyrosine in the FEYNF sequence promoted the formation of dense structural assemblies resembling supramolecular hydrogels, while the FESNY sequence led to the appearance of similar but more loosely organized structures. In contrast, the FEHNF peptide displayed a distinct morphology characterized by micelle-like aggregates with radial projections, highlighting the influence of sequence-specific amino acids on the self-assembly mechanism.

O7. *Investigation of the self-assembly process of the FEYNF peptide by Fourier-transform infrared (FTIR) spectroscopy and fluorescence analysis*

Studies carried out under physiological conditions on the self-assembly mechanism of the FEYNF peptide revealed, through FTIR analysis in the amide I region, that the predominant structure formed is of the β-sheet type. In addition, a fluorescence quenching phenomenon was observed after 10 and 20 minutes, respectively, for two different concentrations of the FEYNF-NH_2 peptide, at 27 μM and 0.5 mM, within the violet–blue spectral range (390–450 nm). These results suggest the gelation properties of the FEYNF peptide.

O8. *In-depth investigation of self-assembly mechanisms and exploration of biomedical applications through in silico studies*

In silico studies revealed that at pH 8.2, intra- and intermolecular π–π interactions are essential for the self-assembly of the FESNF peptide. This peptide favors an "open" conformation that promotes aggregation, and coarse-grained simulations confirmed fibril formation under mildly basic conditions. Moreover, in the case of the FEYNF peptide, molecular docking studies highlighted the role of tyrosine in the formation of hyper-branched structures through π–π interactions with the C-terminal phenylalanine. The protonated dimer (FEYNF@FEYNF(+2)) tends to adopt β-sheet structures, thereby promoting oligomer growth and fibril formation. Additionally, *in silico* simulations indicated that FEYNF can form polyplexes, which are of biomedical relevance for gene therapy applications.

O9. *Dissemination of results through publications and scientific conferences*

The research activity carried out within this doctoral thesis has resulted in the publication of three scientific articles in Web of Science–indexed journals, with a cumulative impact factor of 10.8. Furthermore, the findings were disseminated through the presentation of nine contributions at international conferences and seven contributions at national conferences.

SELECTIVE BIBLIOGRAPHY

- Abbas, M., Ovais, M., Atiq, A., Ansari, T. M., Xing, R., Spruijt, E., Yan, X. (2022). Tailoring supramolecular short peptide nanomaterials for antibacterial applications. *Coordination Chemistry Reviews*, *460*, 214481.
- Accardo, A., Handelman, A. (2022). Optical Polarization-Based Measurement Methods for Characterization of Self-Assembled Peptides' and Amino Acids' Micro- and Nanostructures. *Molecules*, *27*(6), 1802.
- Akter, R., Zou, J., Raleigh, D. P. (2020). Differential effects of serine side chain interactions in amyloid formation by islet amyloid polypeptide. *Protein Science*, *29*(2), 555-563.
- Anand, B. G., Dubey, K., Shekhawat, D. S., Kar, K. (2017). Intrinsic property of phenylalanine to trigger protein aggregation and hemolysis has a direct relevance to phenylketonuria. *Scientific Reports*, *7*(1), 1–9.
- Apostolopoulos, V., Bojarska, J., Chai, T. T., Elnagdy, S., Kaczmarek, K., Matsoukas, J., New, R., Parang, K., Lopez, O. P., Parhiz, H., Perera, C. O., Pickholz, M., Remko, M., Saviano, M., Skwarczynski, M., Tang, Y., Wolf, W. M., Yoshiya, T., Zabrocki, J., Zielenkiewicz, P., AlKhazindar, M., Barriga, V., Kelaidonis, K, Sarasia, E. M., Toth, I. (2021). A Global Review on Short Peptides: Frontiers and Perspectives. *Molecules*, *26*(2), 430.
- Arad, E., Green, H., Jelinek, R., Rapaport, H. (2020). Revisiting thioflavin T (ThT) fluorescence as a marker of protein fibrillation – The prominent role of electrostatic interactions. *Journal of Colloid and Interface Science*, *573*, 87–95.
- Arispe, N., Diaz, J. C., Flora, M. (2008). Efficiency of histidine-associating compounds for blocking the Alzheimer's Aβ channel activity and cytotoxicity. *Biophysical Journal*, *95*(10), 4879–4889.
- Bagińska, K., Makowska, J., Wiczk, W., Kasprzykowski, F., Chmurzyński, L. (2008). Conformational studies of alanine-rich peptide using CD and FTIR spectroscopy. *Journal of Peptide Science*, 14(3), 283–289.
- Barazzouk, S., Daneault, C. (2012). Amino Acid and Peptide Immobilization on Oxidized Nanocellulose: Spectroscopic Characterization. *Nanomaterials* , 2(2), 187–205.
- Barrera, E. E., Zonta, F., Pantano, S. (2021). Dissecting the role of glutamine in seeding peptide aggregation. *Computational and Structural Biotechnology Journal*, 19, 1595–1602.
- Barreto, M. S. C., Elzinga, E. J., Alleoni, L. R. F. (2020). The molecular insights into protein adsorption on hematite surface disclosed by in-situ ATR-FTIR/2D-COS study. *Scientific Reports*, 10(1), 1–13.
- Bernson, D., Mecinovic, A., Abed, M. T., Limé, F., Jageland, P., Palmlöf, M., Esbjörner, E. K. (2020). Amyloid formation of bovine insulin is retarded in moderately acidic pH and by addition of short-chain alcohols. *European Biophysics Journal*, 49(2), 145–153.
- Bortolotti, A., Wong, Y. H., Korsholm, S. S., Bahring, N. H. B., Bobone, S., Tayyab, S., Van De Weert, M., Stella, L. (2016). On the purported "backbone fluorescence" in protein three-dimensional fluorescence spectra. *RSC Advances*, 6(114), 112870–112876.
- Chakraborty, P., Tang, Y., Yamamoto, T., Yao, Y., Guterman, T., Zilberzwige-Tal, S., Adadi, N., Ji, W., Dvir, T., Ramamoorthy, A., Wei, G., Gazit, E. (2020). Unusual Two-Step Assembly of a Minimalistic Dipeptide-Based Functional Hypergelator. *Advanced Materials*, 32(9), 1906043.

- Chen, Y., Tao, K., Ji, W., Kumar, V. B., Rencus-Lazar, S., Gazit, E. (2022). Histidine as a key modulator of molecular self-assembly: Peptide-based supramolecular materials inspired by biological systems. *Materials Today*, 60, 106–127.
- Cojocaru, C., Neamtu, A., Vasiliu, T., Isac, D. L., Pinteala, M. (2021). Molecular Dynamics Simulations and in silico Analysis of Supramolecular Self-assembled Structures. *New Trends in Macromolecular and Supramolecular Chemistry for Biological Applications*, 357–371.
- De Meutter, J., Goormaghtigh, E. (2021). Amino acid side chain contribution to protein FTIR spectra: impact on secondary structure evaluation. *European Biophysics Journal*, 50(3–4), 641–651.
- DiCostanzo, A. C., Thompson, J. R., Peterson, F. C., Volkman, B. F., Ramirez-Alvarado, M. (2012). Tyrosine residues mediate fibril formation in a dynamic light chain dimer interface. *Journal of Biological Chemistry*, 287(33), 27997–28006.
- Emmert, J., Pfluger, M. and Wahl, F. (2004). Influence of Na and K Concentration in Solvents on on mass spectra of peptides in LC/ESI-MS, *Spectroscopy*, 17(12), 646-649.
- Faller, P. (2009). Copper and Zinc Binding to Amyloid-β: Coordination, Dynamics, Aggregation, Reactivity and Metal-Ion Transfer. *ChemBioChem*, 10(18), 2837–2845.
- Gelain, F., Luo, Z., Zhang, S. (2020). Self-Assembling Peptide EAK16 and RADA16 Nanofiber Scaffold Hydrogel. *Chemical Reviews*, 120(24), 13434–13460.
- Guo, M., Gorman, P. M., Rico, M., Chakrabartty, A., Laurents, D. V. (2005). Charge substitution shows that repulsive electrostatic interactions impede the oligomerization of Alzheimer amyloid peptides. *FEBS Letters*, 579(17), 3574–3578.
- Guzmán, F., Aróstica, M., Román, T., Beltrán, D., Gauna, A., Albericio, F., Cárdenas, C. (2023). Peptides, solid-phase synthesis and characterization: Tailor-made methodologies. *Electronic Journal of Biotechnology*, *64*, 27–33.
- Hong, Y., Lau, L. S., Legge, R. L., Chen, P. (2004). Critical self-assembly concentration of an ionic-complementary peptide EAK16-I. *Journal of Adhesion*, 80(10–11), 913–931.
- Insuasty Cepeda, D. S., Pineda Castañeda, H. M., Rodríguez Mayor, A. V., García Castañeda, J. E., Maldonado Villamil, M., Fierro Medina, R., Rivera Monroy, Z. J. (2019). Synthetic Peptide Purification via Solid-Phase Extraction with Gradient Elution: A Simple, Economical, Fast, and Efficient Methodology. *Molecules*, 24(7), 1215.
- Jackson, P., Fisher, K. J., Attalla, M. I. (2011). Tandem Mass Spectrometry Measurement of the Collision Products of Carbamate Anions Derived from CO2 Capture Sorbents: Paving the Way for Accurate Quantitation. *Journal of the American Society for Mass Spectrometry*, 22(8), 1420.
- Jayawarna, V., Richardson, S. M., Hirst, A. R., Hodson, N. W., Saiani, A., Gough, J. E., Ulijn, R. V. (2009). Introducing chemical functionality in Fmoc-peptide gels for cell culture. *Acta Biomaterialia*, 5(3), 934–943.
- **Jitaru, S. C.,** Drochioiu, G. (2023). Mass spectrometric characterization of some gel-forming peptides. *Revue Roumaine De Chimie*, *68*(5), 285-295.
- **Jitaru, S. C.,** Enache, A. C., Drochioiu, G., Petre, B. A., Gradinaru, V. R. (2024). Dendritic-Like Self-assembling Pentapeptide with Potential Applications in Emerging Biotechnologies. *IFMBE Proceedings*, 111, 163–170.
- **Jitaru, S. C.,** Neamtu, A., Drochioiu, G., Darie-Ion, L., Stoica, I., Petre, B. A., Gradinaru, V. R. (2023). A Diphenylalanine Based Pentapeptide with Fibrillating Self-Assembling Properties. *Pharmaceutics*, 15(2), 371.

- Klose, D., Vemulapalli, S. P. B., Richman, M., Rudnick, S., Aisha, V., Abayev, M., Chemerovski, M., Shviro, M., Zitoun, D., Majer, K., Wili, N., Goobes, G., Griesinger, C., Jeschke, G., Rahimipour, S. (2022). Cu^{2+}-Induced self-assembly and amyloid formation of a cyclic D,L-α-peptide: structure and function. *Physical Chemistry Chemical Physics*, *24*(11).
- Konda, M., Bhowmik, S., Mobin, S. M., Biswas, S., Das, A. K. (2016). Modulating Hydrogen Bonded Self–assembled Patterns and Morphological Features by a Change in Side Chain of Third Amino Acid of Synthetic γ- Amino Acid Based Tripeptides. *ChemistrySelect*, 1(11), 2586–2593.
- Lakowicz, J.R. (2006). Principles of fluorescence spectroscopy. Boston, MA: springer US., 27–61.
- Moyer, S. C., VonSeggern, C. E., Cotter, R. J. (2003). Fragmentation of cationized phosphotyrosine containing peptides by atmospheric pressure MALDI/Ion trap mass spectrometry. *Journal of the American Society for Mass Spectrometry*, 14(6), 581–592.
- Munteanu, I. G., Grădinaru, V. R., Apetrei, C. (2022). Development of a Chemically Modified Sensor Based on a Pentapeptide and Its Application for Sensitive Detection of Verbascoside in Extra Virgin Olive Oil. *International Journal of Molecular Sciences*, 23(24), 15704.
- Nathanael, J. G., Gamon, L. F., Cordes, M., Rablen, P. R., Bally, T., Fromm, K. M., Giese, B., Wille, U. (2018). Amide Neighbouring-Group Effects in Peptides: Phenylalanine as Relay Amino Acid in Long-Distance Electron Transfer. *ChemBioChem*, 19(9), 922–926.
- Pan, H. (2008). A non-covalent dimer formed in electrospray ionisation mass spectrometry behaving as a precursor for fragmentations. *Rapid Communications in Mass Spectrometry*, 22(22), 3555–3560.
- Peptide Calculator and Amino Acid Calculator | Bachem. Accesat la 3 iulie 2025: *https://www.bachem.com/knowledge-center/peptide-calculator/*
- Prasad, S., Mandal, I., Singh, S., Paul, A., Mandal, B., Venkatramani, R., Swaminathan, R. (2017). Near UV-Visible electronic absorption originating from charged amino acids in a monomeric protein. *Chemical Science*, 8(8), 5416–5433.
- Restu, W. K., Yamamoto, S., Nishida, Y., Ienaga, H., Aoi, T., Maruyama, T. (2020). Hydrogel formation by short D-peptide for cell-culture scaffolds. *Materials Science and Engineering: C*, 111, 110746.
- Riley, M. K., Vermerris, W. (2017). Recent Advances in Nanomaterials for Gene Delivery—A Review. *Nanomaterials*, 7(5), 94.
- Rodger, A. (2018). UV absorbance spectroscopy of biological macromolecules. *Encyclopedia of Biophysics*, 1–5.
- Ross, A., Sauce-Guevara, M. A., Alarcon, E. I., Mendez-Rojas, M. A. (2022). Peptide Biomaterials for Tissue Regeneration. *Frontiers in Bioengineering and Biotechnology*, 10, 893936.
- Rousseau, F., Schymkowitz, J., Serrano, L. (2006). Protein aggregation and amyloidosis: confusion of the kinds? *Current Opinion in Structural Biology*, 16(1), 118–126.
- Saiani, A., Mohammed, A., Frielinghaus, H., Collins, R., Hodson, N., Kielty, C. M., Sherratt, M. J., Miller, A. F. (2008). Self-assembly and gelation properties of α-helix versus β-sheet forming peptides. *Soft Matter*, 5(1), 193–202.

- Seo, J., Hoffmann, W., Warnke, S., Huang, X., Gewinner, S., Schöllkopf, W., Bowers, M. T., Von Helden, G., Pagel, K. (2016). An infrared spectroscopy approach to follow β-sheet formation in peptide amyloid assemblies. *Nature Chemistry*, 9(1), 39–44.
- Sfragano, P. S., Moro, G., Polo, F., Palchetti, I. (2021). The Role of Peptides in the Design of Electrochemical Biosensors for Clinical Diagnostics. *Biosensors*, 11(8), 246.
- Shattuck, J. E., Waechter, A. C., Ross, E. D. (2017). The effects of glutamine/asparagine content on aggregation and heterologous prion induction by yeast prion-like domains. *Prion*, 11(4), 249–264.
- Sun, B., Tao, K., Jia, Y., Yan, X., Zou, Q., Gazit, E., Li, J. (2019). Photoactive properties of supramolecular assembled short peptides. *Chemical Society Reviews*, 48(16), 4387–4400.
- Sun, S., Yu, C., Qiao, Y., Lin, Y., Dong, G., Liu, C., Zhang, J., Zhang, Z., Cai, J., Zhang, H., Bu, D. (2008). Deriving the probabilities of water loss and ammonia loss for amino acids from tandem mass spectra. *Journal of Proteome Research*, 7(1), 202–208.
- Tian, Y., Viles, J. H. (2022). pH Dependence of Amyloid-β Fibril Assembly Kinetics: Unravelling the Microscopic Molecular Processes. *Angewandte Chemie - International Edition*, 61(48), e202210675.
- Wang, M., Wang, S., Li, B., Tian, Y., Zhang, H., Bai, L., Ba, X. (2021). Synthesis of linear polyglucoside and inhibition on the amyloid fibril formation of hen egg white lysozyme. *International Journal of Biological Macromolecules*, 166, 771–777.
- Yang, J., Luo, G. F. (2023). Peptide-Based Vectors for Gene Delivery. *Chemistry*, 5(3), 1696–1718.
- Yang, S., Wang, M., Wang, T., Sun, M., Huang, H., Shi, X., Duan, S., Wu, Y., Zhu, J., Liu, F. (2023). Self-assembled short peptides: Recent advances and strategies for potential pharmaceutical applications. *Materials Today Bio*, 20, 100644.
- Zaguri, D., Zimmermann, M. R., Meisl, G., Levin, A., Rencus-Lazar, S., Knowles, T. P. J., Gazit, E. (2021). Kinetic and Thermodynamic Driving Factors in the Assembly of Phenylalanine-Based Modules. *ACS Nano*, 15(11), 18305–18311.
- Zapadka, K. L., Becher, F. J., Gomes dos Santos, A. L., Jackson, S. E. (2017). Factors affecting the physical stability (aggregation) of peptide therapeutics. *Interface Focus*, 7(6), 20170030.
- Zelenovskiy, P. S., Shur, V. Y., Nuraeva, A. S., Vasilev, S. G., Vasileva, D. S., Alikin, D. O., Chezganov, D. S., Krasnov, V. P., Kholkin, A. L. (2015). Morphology and Piezoelectric Properties of Diphenylalanine Microcrystals Grown from Methanol-Water Solution. *Ferroelectrics*, 475(1), 127–134.
- Zhang, S., Greenfield, M. A., Mata, A., Palmer, L. C., Bitton, R., Mantei, J. R., Aparicio, C., De La Cruz, M. O., Stupp, S. I. (2010). A self-assembly pathway to aligned monodomain gels. *Nature Materials*, 9(7), 594–601.
- Zhang, Z. (2004). Prediction of Low-Energy Collision-Induced Dissociation Spectra of Peptides. *Analytical Chemistry*, 76(14), 3908–3922.
- Zhou, P., Yuan, C., Yan, X. (2022). Computational approaches for understanding and predicting the self-assembled peptide hydrogels. *Current Opinion in Colloid & Interface Science*, 62, 101645.
- Ziaunys, M., Smirnovas, V. (2019). Emergence of visible light optical properties of L-phenylalanine aggregates. *PeerJ*, 2019(2), e6518.

RESULTS DISSEMINATION

Articles

Scientific articles published in full in Web of Science (WoS) journals with impact factor (at the time of publication):

1. **Jitaru, S.C.,** Enache, A.C., Cojocaru, C., Drochioiu, G., Petre, B.A., Gradinaru, V.R. (2024) Self-Assembly of a Novel Pentapeptide into Hydrogelated Dendritic Architecture: Synthesis, Properties, Molecular Docking and Prospective Applications, *Gels*, 10(2), 86. DOI: 10.3390/gels10020086; I**mpact factor 5.5**, First quartile (Q1 – JIF/AIS)
2. **Jitaru, S.C.,** Neamtu, A., Drochioiu, G., Darie-Ion, L., Stoica, I., Petre, B.A., Gradinaru, V.R. (2023) A diphenylalanine based pentapeptide with fibrillating self-assembling properties, *Pharmaceutics*, 15(2), 371. DOI: 10.3390/pharmaceutics15020371; **Impact factor 4.9**, First/second quartile (Q1 – JIF, Q2 - AIS).
3. **Jitaru, S.C.,** Drochioiu, G. (2023) Mass spectrometric characterization of some gel-forming peptides, *Revue Roumaine de Chimie*, 68(5-6), 285-295. DOI: 10.33224/rrch.2023.68.5-6.12; **Impact factor 0.4**, Fourth quartile (Q4 - JIF/AIS).

   Total impact factor (IF): 10.8

Full-length scientific articles published in conference proceedings volumes:

1. **Jitaru, S.C.,** Enache, A.C., Drochioiu, G., Petre, B.A., Gradinaru, V.R. (2024) Dendritic-like self-assembling pentapeptide with potential applications in emerging biotechnologies, Advances in Digital Health and Medical Bioengineering, *IFMBE Proceedings Springer*, Cham, 111, 105-114,. DOI: 10.1007/978-3-031-62523-7_18